Elsevier Editorial System(tm) for Earth and Planetary Science Letters

Manuscript Draft

Manuscript Number:

Title: The role of melt composition on fluid/melt partitioning of bromine in silicate melts

Article Type: Letters

Keywords: bromine; fluid/melt partitioning; degassing; arc magmas; atmospheric chemistry

Corresponding Author: Dr. Anita Cadoux, Ph.D

Corresponding Author's Institution: Université d'Orléans

First Author: Anita Cadoux, Ph.D

Order of Authors: Anita Cadoux, Ph.D; Giada Iacono-Marziano; Bruno Scaillet; Alessandro Aiuppa; Tamsin A Mather; David M Pyle; Etienne Deloule; Emanuela Gennaro; Antonio Paonita

Abstract: Volcanogenic halogens, in particular bromine, play an important role in the ozone depletion of the atmosphere. Understanding bromine behaviour in magmas is therefore crucial to properly evaluate the contribution of volcanic eruptions to atmospheric chemistry and their environmental impact. To date, bromine partitioning between silicate melts and the gas phase is very poorly constrained, with the only relevant experimental studies limited to investigation of synthetic melt with silicic compositions. Here, we perform fluid/melt partitioning experiments using natural silicate glasses with mafic, intermediate and silicic compositions. For each composition, experiments were run with various Br contents in the initial fluid (H2O-NaBr), at T - P conditions representative of magmatic reservoirs in volcanic arc contexts (100-200 MPa, 900-1200°C). The resulting fluid/melt partition coefficients (DBrf/m) are: 5.0 ± 0.3 at 1200°C -100 MPa for the basalt, 9.1 ± 0.6 at 1060°C - 200 MPa for the andesite and 20.2 ± 1.2 at 900°C - 200 MPa for the rhyodacite. Our experiments show that DBrf/m increases with increasing SiO2 content of the melt (as for chlorine) and suggest that it is also sensitive to melt temperature (increase of DBrf/m with decreasing temperature). We develop a simple model to predict the S-Cl-Br degassing behaviour in mafic systems, which accounts for the variability of S-Cl-Br compositions of volcanic gases from Etna and other mafic systems, and shows that coexisting magmatic gas and melt evolve from S-rich to Cl-Br rich upon increasing degree of degassing. We also report first Br contents for melt inclusions from Etna, Stromboli, Merapi and Santorini eruptions and calculate the mass of bromine available in the magma reservoir prior to the eruptions under consideration. The discrepancy that we highlight between the mass of Br in the co-existing melt and fluid prior to the Merapi 2010 eruption (433 and 73 tons, respectively) and the lack of observed BrO (from space) hints at the need to investigate further Br speciation in 'ash-rich' volcanic plumes. Overall, our results suggest that the Br yield into atmosphere of cold and silicic magmas will be much larger than that of those which are hotter and more mafic.

Highlights

- First bromine partition experiments performed with natural silicate glasses
- First Br fluid/melt partition coefficients ($D_{Br}^{f/m}$) on mafic and intermediate compositions
- $D_{Br}^{f/m}$ increases with SiO_2 content of the melt, from basalt to rhyodacite compositions
- Our results suggest that $D_{Br}^{f/m}$ is also sensitive to melt temperature
- We present the first Br data in melt inclusions from Etna, Stromboli, Merapi and Santorini volcanoes

The role of melt composition on fluid/melt partitioning of bromine in silicate melts

Anita Cadoux[a,b,c], Giada Iacono-Marziano[a,b,c], Bruno Scaillet[a,b,c], Alessandro Aiuppa[d,e], Tamsin A. Mather[f], David M. Pyle[f], Etienne Deloule[g], Emanuela Gennaro[a,b,c,e], Antonio Paonita[d]

[a] Université d'Orléans, ISTO, UMR 7327, 45071, Orléans, France
[b] CNRS, ISTO, UMR 7327, 45071 Orléans, France
[c] BRGM, ISTO, UMR 7327, BP 36009, 45060 Orléans, France
[d] Istituto Nazionale di Geofisica e Vulcanologia, Sezione di Palermo, Italy
[e] DiSTeM, Università di Palermo, Italy
[f] Department of Earth Science, University of Oxford, Oxford OX1 3AN, United Kingdom
[g] CNRS, CRPG, Université de Lorraine, UMR 7358, BP 20, 54501 Vandoeuvre-lès-Nancy Cedex, France

Corresponding author: Anita Cadoux

Now at:

Université Paris Sud
UMR Géosciences Paris Sud (GEOPS)
Rue du Belvédère
Bât. 504
Orsay, F-91405, France

E-mail: anita.cadoux@u-psud.fr

Manuscript for submission to *EPSL*

Abstract

Volcanogenic halogens, in particular bromine, play an important role in the ozone depletion of the atmosphere. Understanding bromine behaviour in magmas is therefore crucial to properly evaluate the contribution of volcanic eruptions to atmospheric chemistry and their environmental impact. To date, bromine partitioning between silicate melts and the gas phase is very poorly constrained, with the only relevant experimental studies limited to investigation of synthetic melt with silicic compositions. Here, we perform fluid/melt partitioning experiments using natural silicate glasses with mafic, intermediate and silicic compositions. For each composition, experiments were run with various Br contents in the initial fluid (H_2O-NaBr), at T - P conditions representative of magmatic reservoirs in volcanic arc contexts (100-200 MPa, 900-1200°C). The resulting fluid/melt partition coefficients ($D_{Br}^{f/m}$) are: 5.0 ± 0.3 at 1200°C -100 MPa for the basalt, 9.1 ± 0.6 at 1060°C - 200 MPa for the andesite and 20.2 ± 1.2 at 900°C - 200 MPa for the rhyodacite. Our experiments show that $D_{Br}^{f/m}$ increases with increasing SiO_2 content of the melt (as for chlorine) and suggest that it is also sensitive to melt temperature (increase of $D_{Br}^{f/m}$ with decreasing temperature). We develop a simple model to predict the S-Cl-Br degassing behaviour in mafic systems, which accounts for the variability of S-Cl-Br compositions of volcanic gases from Etna and other mafic systems, and shows that coexisting magmatic gas and melt evolve from S-rich to Cl-Br rich upon increasing degree of degassing. We also report first Br contents for melt inclusions from Etna, Stromboli, Merapi and Santorini eruptions and calculate the mass of bromine available in the magma reservoir prior to the eruptions under consideration. The discrepancy that we highlight between the mass of Br in the co-existing melt and fluid prior to the Merapi 2010 eruption (433 and 73 tons, respectively) and the lack of observed BrO (from space) hints at the need to investigate further Br speciation in ‘ash-rich’ volcanic plumes.

Overall, our results suggest that the Br yield into atmosphere of cold and silicic magmas will be much larger than that of those which are hotter and more mafic.

Keywords: bromine, fluid/melt partitioning, degassing, arc magmas, atmospheric chemistry

1. Introduction

Volcanic degassing is an important process in sustaining the composition of Earth's atmosphere (e.g., Mather et al., 2003; Gaillard and Scaillet, 2014). Whilst much progress has been made constraining global volcanic fluxes, uncertainties remain regarding the emissions of the key halogen species, especially the trace Br- and I-bearing species (Pyle and Mather, 2009). However, improvements in remote sensing techniques and analytical techniques, and their use on an increasing number of active volcanoes, have provided new data on the concentrations of these minor species in volcanic gases (e.g., Gerlach, 2004; Aiuppa et al., 2005; Aiuppa, 2009; Bobrowski et al., 2015), which in turn can be used to better constrain their global fluxes to the atmosphere (Pyle and Mather, 2009). Bromine has received particular attention over the last decade, owing to its important role in atmospheric chemistry in general (e.g., Oppenheimer et al., 2006; Roberts et al., 2009; 2014) and ozone depletion in the troposphere and stratosphere in particular (von Glasow et al., 2009; Kutterolf et al., 2013; Cadoux et al., 2015). Global compilations show that Br sources and sinks are not strictly balanced, hinting at a missing natural source of Br (Montzka et al., 2011). The direct detection of HBr and BrO in volcanic plumes (Bobrowski et al., 2003; Aiuppa et al., 2005) showed that volcanic activity may be one such a source.

The correct evaluation of the contribution of past volcanic eruptions to atmosphere chemistry depends on our ability to evaluate Br behaviour in magmas, in particular its partitioning between silicate melt and gas phases. So far, only a few experimental studies have been performed on this topic, and have investigated Br behaviour in synthetic melt compositions, albitic to rhyolitic (Bureau et al., 2000; Bureau and Métrich, 2003). However, natural silicate melt compositions can depart significantly from such model systems, in particular by having elevated contents of Fe, Mg or Ca, which can complex with halogens thereby enhancing their solubility in silicate melts, as shown for Cl (Webster et al., 1999). There is thus a need to

evaluate the role of melt composition on Br behaviour in magmas, which is the main motivation of the present study. To that end, we have performed fluid/melt partitioning experiments on natural basalt, andesite and rhyodacite compositions under P-T-H_2O-redox storage conditions relevant to arc magmas. Using the partition coefficient determined for the mafic composition, we develop a simple model to predict the S-Cl-Br degassing behaviour in mafic systems. We also measure Br contents of melt inclusions from Etna, Stromboli, Merapi and Santorini eruptions and estimate the mass of bromine in the pre-eruptive magmas, this allows us to address the atmospheric contribution of open-vent mafic volcanoes versus that of intermediate-silicic volcanoes.

2. Fluid/melt partitioning experiments

2.1 Starting material

The selected starting materials are natural volcanic rocks: a hawaiitic basalt from a 2002 Etna eruption (Lesne et al., 2011a, b; Iacono-Marziano et al., 2012), a calc-alkaline andesite and a rhyodacite from the Santorini Upper Scoria-2 (USC-2) and Minoan eruptions, respectively (Cadoux et al., 2014). The whole-rocks were crushed and ground in an agate mortar. About 10 g of the powders were melted twice (with grinding in between), to ensure homogenization, in a platinum crucible at 1400 °C - 1 atm for 3-4 hours in a piezoceramic oven, and quenched in cold water. The resulting dry glasses were then reduced to powder and constituted the starting material for both (i) bromine standard glasses synthesis (Cadoux et al., 2017) used to calibrate bromine analyses (section 3) and (ii) partitioning experiments. The compositions of the starting glasses are given in Table 1.

2.2 Experimental procedure

Experiments were performed in an Internally Heated Pressure Vessel equipped with a rapid quench device at the Institut des Sciences de la Terre d'Orléans (ISTO, Orléans, France). The chosen T-P-fO_2 experimental conditions are representative of those in shallow crustal reservoirs in volcanic arc contexts (Martel et al., 1999; Di Carlo et al., 2006; Cadoux et al., 2014; Kahl et al., 2015) and are reported in Table 2: 900, 1060 and 1200°C, 100 and 200 MPa, and fO_2 estimated around the Ni-NiO (NNO) buffer, on the basis of the partial pressure of H_2 imposed in the vessel (~2 bars; Di Carlo et al., 2006; Cadoux et al., 2014).

About 50 to 100 mg of glass powder was loaded into Au or Au-Pd capsules (2.5 mm internal diameter, 20-30 mm in length) together with 3-8 mg of a solution composed of distilled water and dissolved NaBr salt. These amounts of solution (6-10 wt%) ensure the attainment of fluid saturation of the silicate melts at the investigated T-P conditions. Different solutions with Br contents between 0.1 and 14 wt% Br were employed. The runs lasted between 24 and 92 hours, depending on the temperature (Table 2) and were terminated by drop quench (Di Carlo et al., 2006). Upon opening the capsules, hissing and fluid escape was observed, indicating the presence of excess fluid, and thus that fluid saturation was achieved at the target P-T conditions. All runs produced crystal-free glasses, those of rhyodacitic composition being rich in fluid inclusions (Fig. A.1 in Appendix).

3. Analytical techniques

3.1. Major element analysis

Experimental glasses and natural melt inclusions were analysed for their major elements by electron microprobe (EMP) using the joint ISTO-BRGM SX-Five microbeam facility (Orléans, France). The operating conditions were: 15 kV accelerating voltage, 4-6 nA beam

current, 10 seconds counting time on peaks, 5 seconds on background, defocused beam to minimize alkali migration of 20 µm for experimental glasses, and 6-10 µm for melt inclusions. Between 5 and 10 analyses were performed on each charge.

3.2. Volatile analysis

Br abundances in the experimental glasses were determined either by Laser Ablation Inductively Coupled Plasma Mass Spectrometry (LA-ICP-MS) or with a Secondary Ion Mass Spectrometer (SIMS), using Br glass standards synthesized with the same starting compositions as those used for the partitioning experiments presented here (Table 1, Cadoux et al., 2017). LA-ICP-MS has been shown to be a technique suited to analyse Br contents of hundreds to thousands ppm in experimental glasses, while SIMS and synchrotron X-ray fluorescence (SR-XRF) are more appropriate techniques for lower Br contents (Cadoux et al., 2017). Moreover, the spatial resolutions of SIMS and SR-XRF are significantly higher than that of LA-ICP-MS (Cadoux et al., 2017), we therefore analysed bromine contents in melt inclusions from Santorini, Merapi and Etna volcanoes by SIMS and SR-XRF.

The abundance of water dissolved in most of the experimental glasses was determined by SIMS.

3.2.1. Bromine analysis by LA-ICP-MS

LA-ICP-MS analyses were performed at the Istituto Nazionale di Geofisica e Vulcanologia (INGV, Palermo, Italy). The laser used is a Compex Pro 102, 193 nm ArF excimer laser mounted on an ablation system GeoLas Pro, which is connected to an Agilent 7500ce ICP-MS. Analyses were done on polished glass chips set in epoxy resin.

Analyses were performed with a fluency (i.e., the energy density of the laser on the sample surface) of 15 J/cm^2, and a pulse energy of 100 mJ. The samples were ablated during ~50

seconds on a 90 µm diameter area, with a pulse repetition rate of 10 Hz. Three to ten chromatograms were collected for every sample, to check sample homogeneity. With this configuration, Br contents of >100 ppm are quantifiable with accuracy within 20% (Cadoux et al., 2017).

Data reduction was performed using GLITTER™ software (Griffin et al., 2008), using ^{24}Mg as the reference element (Mg contents from EMP analyses), and in-house bromine glass standards B3000 and B6000 (with 2694 and 5968 ppm Br, respectively; Cadoux et al., 2017), as external standards.

3.2.2. Bromine analysis by SIMS

Polished chips of experimental glasses were set into indium and coated with gold, while individual crystals from Santorini Minoan eruption, Merapi 2010 eruption and Etna 2006 eruption were mounted in epoxy resin, polished and coated with gold for melt inclusion analysis.

Analyses were conducted at the Centre de Recherches Pétrographiques et Géochimiques (CRPG, Nancy, France) with a Cameca 1280 HR2. The Cs^+ primary ion beam was accelerated at 10 kV with an intensity of 5 nA, and focused on a 15 µm diameter area. The electron gun was simultaneously used for charge compensation. Negative secondary ions were extracted with a 10 kV potential, and the spectrometer slits set for a mass resolving power (MRP = M/ΔM) of ~20,000. A single collector (EM) was used in ion-counting mode, and the spectrum scanned by peak jumping. Each analysis consisted of 8 or 6 successive cycles. Each cycle began with background measurement at the mass 75.8, followed by $^{28}Si^{16}O_3^-$ (75.963 amu), $^{30}Si^{16}O_3^-$ (77.959 amu), $^{79}Br^-$ and $^{81}Br^-$, with measurement times of 4, 4, 4, 10 and 30 s, respectively (waiting time of 2 s). More details about the analytical configuration can be found in Cadoux et al. (2017).

We used three different sets of in-house bromine glass standards (Cadoux et al., 2017): a basaltic set containing 1 to 6,000 ppm Br, an andesitic set containing 10 to 1,000 ppm Br, and a rhyodacitic set containing 10 to 5,000 ppm Br.

The bromine content of the samples was calculated using the measured $^{81}Br/^{28}SiO_3$ and known Br (ppm)/SiO_2 (wt%) ratios of the standards. Br contents in the standards were determined by instrumental neutron activation analysis (INAA) and SiO_2 by electron microprobe (Cadoux et al., 2017).

The three glass sets define distinct linear calibration curves with slopes decreasing with increasing degree of melt polymerization (Cadoux et al., 2017). The equation of the calibration lines passing through zero is:

$$\left(\frac{^{81}Br}{^{28}SiO_3}\right) = a\left(\frac{Br}{SiO_2}\right)$$

where the slope a is a function of SiO_2 content.

The maximum internal error on the $^{81}Br/^{28}SiO_3$ ratio was 15% but was generally < 5%.

3.2.3. Br analysis by SR-XRF

Bromine in Etna and Stromboli melt inclusions was analysed via SR-XRF at the UK national synchrotron facility, Diamond Light Source (Didcot, Oxfordshire), on I18, the Microfocus Spectroscopy beamline. Analyses were performed on polished olivine-hosted melt inclusions set in epoxy resin, using a beam of ~5×5 μm^2 and an analysis time of 120 s (details in Cadoux et al., 2017). Fluorescence spectra were processed by PyMca (Solé et al., 2007), by identifying the K-lines of Br and applying an iterative peak fitting procedure to quantify the net peak areas free of background and interference from other elements.

3.2.4. Water analysis by SIMS

The analysis of water dissolved in the experimental glasses was performed on the CRPG Cameca 1280 HR2. Spot analyses of secondary ions ^{17}O, $^{16}O^{1}H$, ^{18}O, ^{29}Si, ^{30}Si were obtained using a 3 nA, 20 µm diameter primary beam of Cs^{+} ions. The electron gun was simultaneously used for charge compensation. The measurements were made at a mass resolution of ~7,700 to separate $^{17}O^{-}$ and $^{16}O^{1}H^{-}$. An energy filtering was set at +30 ±10 eV in moving the energy slit off axis, to minimize both matrix effect and instrumental background. A 10 × 10 µm raster was used for 1 minute prior to analysis at each spot in order to pre-sputter through the gold coat and remove surface contamination. The beam position in the field aperture and the magnetic field centering was checked before each measurement. Each analysis on one spot consisted of 18 cycles of measurements, with counting times and switching times of 3 and 1 s respectively at each peak.

Concentrations of H_2O were calculated using a best-fit quadratic polynomial regression to count-rate ratios (normalized to ^{30}Si) versus variable known concentration ratios (referenced to wt% SiO_2) of experimental glass standards of basaltic (sample N72, Kamtchatka; Shishkina et al., 2010), trachy-andesitic (sample TAN25, Tanna Island, Vanuatu; Metrich & Deloule, 2014), dacitic and rhyolitic (Pinatubo, Philippines; Scaillet & Evans, 1999) compositions, with H_2O contents ranging from 0 to ~6 wt%.

4. Results

Average major element compositions of experimental glasses and melt inclusions are presented in Tables 3 and 4, respectively. The compositions of the experimental products do not show any significant difference with the starting glass compositions.

4.1. H_2O and Br dissolved in experimental glasses

The concentrations of both H_2O and Br dissolved in quenched glasses are reported in Table 2. Melt water contents (H_2O_{melt}) vary between 2.9 up to 7.3 wt%, encompassing the range of pre-eruptive H_2O_{melt} of arc magmas (e.g., Scaillet et al., 1998; Di Carlo et al., 2006; Cadoux et al., 2014). Bromine concentrations range from 69 (M4-RD1; Table 2) to 9112 ppm (M2-B), comparable to the range explored in previous experimental studies (Bureau et al., 2000; Bureau and Métrich, 2003). Repeat analyses of either H_2O (n = 5-7) or Br (n = 3-10) in quenched glasses show them to be homogeneous within analytical uncertainty.

4.2. Fluid/melt bromine partitioning

Assessment of the partition coefficients requires the calculation of the ratio between Br concentration in coexisting fluid and silicate melt at the experimental conditions. Whereas the amount of Br dissolved in the melt ($[Br]_{melt}$) was directly analysed (by SIMS or LA-ICP-MS in run glasses, section 3; referred to as '[Br] measured in quenched glass' in Table 2), the Br amount of the coexisting fluid phase ($[Br]_{fluid}$) was determined by mass balance, knowing the original bulk Br content (the amount of Br loaded in the capsule as H_2O+NaBr solution; hereafter [Br°]), the measured amount of Br dissolved in the glass ($[Br]_{melt}$), and assuming that the difference between these two figures represents the amount of Br left over for the fluid phase. The amount of Br in the fluid ($[Br]_{fluid}$) was then determined by calculating the fluid lost using mass balance based on the measurements of the starting and final compositions of the experimental charge (details in Appendix: Table A.1). The results are listed in Table 2 and displayed on Figures 1 to 5.

The basaltic products of runs #1 to 3 performed at 1200°C, 100 MPa, with various [Br°] contents show a linear relationship between the measured $[Br]_{melt}$ and the calculated $[Br]_{fluid}$ (Fig. 1). Linear regression forced through zero yields a $D_{Br}^{f/m} = 5.0 \pm 0.3$ for the basaltic

composition. At the same T-P-[Br°] conditions (experiment #3; Table 2), the $D_{Br}^{f/m}$ increases steadily from basalt ($D_{Br}^{f/m}$ = 4.6), to andesite ($D_{Br}^{f/m}$ = 6.4), to rhyodacite ($D_{Br}^{f/m}$ = 11.3). At 1060°C, 200 MPa, ~NNO (Fig. 2), experiments on andesite and rhyodacite melts yields linear trends between $[Br]_{melt}$ and [Br°] (Fig. 2a) or $[Br]_{fluid}$ (Figs. 2b and 2c). Linear regression of the latter data forced through zero yields a $D_{Br}^{f/m}$ = 9.1 ± 0.6 for andesite, and a $D_{Br}^{f/m}$ = 13.9 ± 0.6 for rhyodacite. At 900°C, 200 MPa, (Fig. 3), the same pattern is again observed resulting in a $D_{Br}^{f/m}$ = 20.2 ± 1.2 for rhyodacite, slightly higher than that of Bureau et al. (2000) for albitic melts (17.5 ± 0.6).

The experiments show a two fold increase of $D_{Br}^{f/m}$ from basalt to rhyolite melts at 1200°C (Fig. 4). The same trend of an increase of $D_{Br}^{f/m}$ with SiO_2 is noted at 1060°C, with a slightly higher slope. At 900°C, we did not work on basaltic/andesitic compositions because of their extensive crystallization (which would have driven the residual liquids toward higher SiO_2 content). The data on the silicic composition of the present work, along with those of Bureau et al. (2000) (Fig. 4), suggest a similar trend of increasing $D_{Br}^{f/m}$ with increasing SiO_2 at 900°C. Figure 4 also suggests a general trend of an increase in $D_{Br}^{f/m}$ as temperature decreases, at least for more silicic compositions. For instance, for rhyolitic melts (70 wt% SiO_2), a linear extrapolation of our data set ($D_{Br}^{f/m} = -0.0299 \times T(°C) + 46.576$, $r^2 = 0.97$) yields a $D_{Br}^{f/m}$ = 26 at 700°C (Fig. 5).

We did not attempt to explore the effect of pressure in a systematic way. Previous work has shown that $D_{Br}^{f/m}$ strongly increases as pressure decreases, from about 20 at 200 MPa up to over 300 at near atmospheric pressure in silicic melts (synthetic haplogranitic composition; Bureau et al., 2010). In contrast, our experiment at 100 MPa (experiment #3) does not show any significant increase in $D_{Br}^{f/m}$, with $D_{Br}^{f/m}$ being instead generally lower than those at 200 MPa (experiments #4 and #5; Table 2). However, the fact that temperatures between our 100 and 200 MPa runs are different, does not allow us to make definitive conclusions on this

aspect. We suggest that our results should be used to model degassing processes in the crustal reservoir and not for simulating decompression processes between the reservoir and surface.

4.3. Br contents in melt inclusions

Table A.2 reports the Br contents of melt inclusions from (i) basaltic magmas erupted at Mount Etna and Stromboli, (ii) the andesitic magma erupted in 2010 at Mount Merapi, and (iii) the rhyodacitic magma of the 1613 BC Minoan eruption of Santorini volcano. Melt inclusions from Mt. Etna and Stromboli are hosted by olivine crystals, while those from Mt. Merapi and Santorini volcano are in pyroxenes and plagioclase crystals, respectively.

Br abundance ranges from 2.5 to 10 ppm, without any clear correlation with melt inclusion composition.

5. Discussion and applications

5.1. Halogen behaviour

This section aims to place our novel Br partitioning data in the wider framework of halogen behaviour. Hereafter, we provide a brief, non-exhaustive, state of the art about chlorine, fluorine and iodine partitioning behaviours and make comparisons with bromine.

Many studies have been dedicated to understanding the partitioning behaviour of halogens between fluids and silicate melts (e.g., Webster, 1990; Webster and Holloway 1990; Webster 1992a,b; Webster et al. 1999; Signorelli and Carroll, 2000; Bureau et al., 2000; Botcharnikov et al., 2004, 2007, 2015; Dolejs and Baker 2007a,b; Alletti, 2008; Stelling et al. 2008; Chevychelov et al., 2008b; Webster et al., 2009; Borodulin et al., 2009; Alletti et al. 2009, 2014; Beermann 2010; Baker and Alletti 2012; Zajacz et al. 2012; Webster et al., 2014; Beermann et al., 2015). Nevertheless, most of these studies have focused on chlorine, mainly

because of its importance as a ligand for ore metals (e.g., Carroll and Webster, 1994; Aiuppa et al., 2009).

5.1.1 General behaviour

Chlorine partitions preferentially into fluids relative to melts for the vast majority of terrestrial magmas at shallow-crustal pressure and temperature conditions, due to its highly solubility in aqueous and aqueous-carbonic fluids (e.g., Webster et al., 2017 and references therein). The few partitioning experiments performed with bromine and iodine show a similar behaviour (Bureau et al., 2000; this study). In contrast, fluorine concentrations in aqueous and aqueous-carbonic fluids at magmatic conditions are much lower than those of the other halogens (e.g., Carroll and Webster, 1994), and can be therefore enriched in the silicate melt with respect to the fluid phase (e.g., Webster, 1990; Webster and Holloway 1990).

5.1.2 The effect of melt composition

In this study, we show that the partitioning of bromine between aqueous fluid and melt appears to be influenced by the melt composition (Figs. 1, 2, 4). We estimate $D_{Br}^{f/m}$ of 4.6, 6.4 and 11.3 for basaltic, andesitic and rhyodacitic compositions respectively, with [Br°] = 2.4 wt.%, at 1200°C, 100 MPa and fO_2 close to NNO (exp. #3, Table 2). This relationship between melt composition and Br partitioning is consistent with the higher Br solubility in melts with lower SiO_2 observed by Bureau and Métrich (2003). The recent study of Cochain et al. (2015) on Br speciation in hydrous alkali silicic melts at high pressure (up to 7.6 GPa) confirms this trend. Similarly, several studies have demonstrated the strong effect of melt composition on fluid-melt partitioning of chlorine (Webster 1992a,b; Webster et al. 1999; Stelling et al. 2008). Like $D_{Br}^{f/m}$, $D_{Cl}^{f/m}$ also increases with increasing SiO_2 contents of the melts (i.e., with increasing melt polymerization and thus decreasing Br and Cl solubility in

melt; e.g., Webster, 1992a,b; Signorelli and Carroll, 2000; Botcharnikov et al., 2004; Webster, 2004; Webster et al., 2006; Webster et al., 2009). Most experimental values of $D_{Cl}^{f/m}$ for basaltic systems are <10 (Stelling et al 2008; Beermann 2010; Baker and Alletti 2012), but Alletti et al. (2009) observed $D_{Cl}^{f/m}$ of 8-34 in trachybasaltic melt in equilibrium with aqueous fluids at fO_2 near NNO. Values of $D_{Cl}^{f/m}$ for intermediate (andesitic and phonolitic) and silicic melts exceed those for mafic melts (e.g., Webster et al. 1999; Stelling et al., 2008; Chevychelov et al., 2008b; Alletti et al., 2009; Beermann, 2010; Beermann et al., 2015); with values >160 determined for silicic melts at 200 MPa (Webster, 1992a). On the contrary, F dissolves at higher concentrations in SiO_2-poor melts than in SiO_2-rich ones. Values of $D_F^{f/m}$ for trachybasaltic melts coexisting with aqueous fluids range from ca. 3 to 38 (Alletti, 2008; Chevychelov et al., 2008b), while those for more-polymerized silicic melts are typically well below unity (Webster, 1990; Webster and Holloway 1990; Dolejs and Baker 2007a,b; Borodulin et al., 2009).

5.1.3 Temperature and pressure effects

Our data suggest that $D_{Br}^{f/m}$ is sensitive to melt temperature (increase of $D_{Br}^{f/m}$ with decreasing temperature; Figs. 4 and 5), though more experiments are required to confirm this trend. Currently there are insufficient data available to constrain the temperature effect for the other halogens. The few existing data concern Cl in phonolitic and trachybasaltic melts and suggest that there is no strong influence of temperature (Chevychelov et al., 2008a; Stelling et al., 2008).

We do not systematically investigate the effect of pressure on $D_{Br}^{f/m}$. Experiments conducted on trachybasaltic melts coexisting with aqueous fluids suggest that $D^{f/m}$ of fluorine increases with increasing pressure (Alletti, 2008; Chevychelov et al., 2008b), while available data for

chlorine show no clear pressure effect on $D_{Cl}^{f/m}$ for most compositions and contrasting effects for phonolitic ones (Signorelli and Carroll, 2000; Baker and Alletti, 2012; Alletti et al. 2014). We conclude that more systematic experiments are necessary for all halogens to assess the effect of pressure and temperature on their fluid/melt partitioning, in order to interpret degassing processes of ascending and cooling magmas comprehensively.

5.1.4 Effect of fluid composition

Experiments with trachybasaltic melts coexisting with aqueous fluids have shown that the addition of CO_2 to the system leads significant reductions of $D^{f/m}$ of fluorine.

The effect of fluid composition on Cl partitioning in chemically complex C-O-H-S-Cl fluids has been studied (Botcharnikov et al. 2004; Webster et al. 2003; Botcharnikov et al., 2007; Alletti et al., 2009; Beermann 2010, Zajacz et al. 2012; Webster et al., 2014) but requires further investigation and to be extended to the other halogens.

5.2. S-Cl-Br degassing behaviour in mafic magma systems

Our partition coefficients for Etnean melts set the basis for initializing the first basic models to evaluate Br degassing behaviour in mafic systems. Our aim is to derive model-based evidence for Br abundance in magmatic gases coexisting with mafic melts at shallow crustal conditions, and to compare this with available information on the measured compositions of volcanic gases, which are the ultimate product of magmatic degassing. Figure 6a shows a selection of volcanic gas plume compositions (in the S-Cl-Br system) from some open-vent mafic volcanoes (for data provenance, see caption of Figure 6). The wide range of volcanic gas S/Br compositions observed points to a mechanism fractionating Br, relative to sulphur, during magmatic degassing. In comparison, volcanic gases exhibit a far more restricted range of Cl/Br ratios (see Fig. 6a and Gerlach, 2004; Aiuppa et al, 2005, 2009;

Webster et al., 2017), which suggests that less Cl/Br fractionation takes place during degassing. We consider below our new Br partitioning data, in tandem with previous information on S and Cl from the literature, to provide a simple model verification for these volcanic gas-based inferences.

Rigorous quantitative calculation of magmatic gas compositions would require a theoretical and/or empirical model that describes solubilities, vapour-melt partition coefficient, and diffusivities of all involved volatiles over the range of P-T-X conditions experienced by magmas upon ascent, storage, and eruption. Such quantitative information is increasingly available for S (see review of Baker and Moretti, 2011), still limited for Cl (Webster et al., 1999, 2015, 2017), but virtually absent for Br. Given this limitation, we base our model calculations on a modified version of the empirical degassing model of Aiuppa et al. (2002) and Aiuppa (2009). The original model described the evolution of the SO_2-HCl-HF magmatic gas phase exsolved during progressive degassing of a basaltic magma, using a Rayleigh-type open-system degassing model assumption, and with constant S, Cl and F melt-vapour partition coefficients. Based on fair agreement between model results and volcanic gas compositions, it was concluded that a Rayleigh-type open-system process could suitably reproduce the relatively shallow exsolution of halogens from basaltic magmas (Métrich and Wallace, 2008; Métrich et al., 2001, 2004, 2010; Spilliaert et al., 2006; Edmonds et al., 2009; Webster et al., 1999, 2015).

Here we adapt and extend the methodology of Aiuppa (2009) to bromine, and develop a simple model to account for the variability of S-Cl-Br compositions of volcanic gases (Fig. 6a). We use similar sets of Rayleigh-type open-system equations as in Aiuppa (2009) but, contrarily to previous work, we do not derive vapour/melt partition coefficients using an empirical best-fit procedure to volcanic gas data, but rather use independent information (from Alletti et al., 2009; Aiuppa, 2009; and this work) (see below).

406 We use equations (1) and (2) to calculate the evolving S/Cl and S/Br (molar) ratios in the
407 magmatic gas phase produced upon increasing extents of degassing of a mafic silicate melt:

408 $$\left(\frac{S}{Cl}\right)_{gas} = \left(\frac{S}{Cl}\right)_{melt_0} \cdot \frac{D_S}{D_{Cl}} \cdot R^{\left(1-\frac{D_{Cl}}{D_S}\right)} \quad (1)$$

409 $$\left(\frac{S}{Br}\right)_{gas} = \left(\frac{S}{Br}\right)_{melt_0} \cdot \frac{D_S}{D_{Br}} \cdot R^{\left(1-\frac{D_{Br}}{D_S}\right)} \quad (2)$$

410 where $\left(\frac{S}{Cl}\right)_{gas}$ and $\left(\frac{S}{Br}\right)_{gas}$ are the molar volatile ratios in the gas phase; $\left(\frac{S}{Cl}\right)_{melt_0}$ and
411 $\left(\frac{S}{Br}\right)_{melt_0}$ are the original volatile ratios in the parental (un-degassed) melt; D_S, D_{Cl} and D_{Br} are
412 the vapour/melt (molar) partition coefficients for the three volatiles; and R is the residual
413 fraction of sulphur in the melt (ranging from 1 at onset of degassing to 0 if S is totally
414 exsolved from the melt).

415 To resolve the model equations, $\left(\frac{S}{Cl}\right)_{melt_0}$ and $\left(\frac{S}{Br}\right)_{melt_0}$ are here set at 1.7 and 1320,
416 respectively, from the characteristic S (0.27 wt %), Cl (0.18 wt. %) and Br (5.1 ppm) contents
417 in our most primitive, un-degassed glass inclusions from Etna (inclusion E2 from the 2001
418 eruption; Table A.2). For the vapour-melt partition coefficients, we use our results on Etnean
419 melts for Br ($D_{Br}^{f/m}$ = 5.0; Fig. 1) and those of Alletti et al. (2009) for Cl ($D_{Cl}^{f/m}$ = 8.6),
420 obtained at the same pressure (100 MPa), temperature (1200°C), redox conditions (NNO) and
421 melt composition. These conditions are appropriate to describe halogen behaviour at shallow
422 crustal conditions including shallow degassing, in view of the minor pressure-dependence of
423 halogen vapour-melt partition coefficients (Alletti et al., 2009). For S, we adopt a vapour-melt
424 partition coefficients of 78 based on the results of Aiuppa (2009), who found that volcanic gas
425 measurements from Etna and several mafic arc volcanoes worldwide can satisfactorily be

426 reproduced with a D_S/D_{Cl} ratio (ratio between vapour/melt partition coefficients) of 9. Our
427 inferred $D_S = 78$ agrees well with results obtained from S thermodynamic modelling (Moretti
428 and Ottonello, 2005) of Etna-like melts at $P \leq 100$ MPa, ~ NNO and ~ 3 wt.% H_2O (Aiuppa et
429 al., 2007), and is also reasonably consistent with S-bearing experiments performed on Etnean
430 melts (Lesne et al., 2015), which give a range of D_S between 25 and 100 depending on P-T-
431 fO_2 conditions. We argue that our inferred D_S of 78, derived from empirical fitting of
432 hundreds of volcanic gas data, is suitable to describe an "averaged" S degassing behaviour in
433 mafic systems, integrating together the complex S dependences on T, P, redox and melt
434 composition.
435 With these numbers, and with R varied from 1 (start of degassing) to 0 (complete S exsolution
436 from the melt), the magmatic *vapour model line* shown in Figure 6a is obtained. The evolving
437 volatile composition of the coexisting melt is obtained by mass balance, and is illustrated by
438 the *melt model line* (solid red line) in Fig. 6b.
439 Our model results predict that the coexisting magmatic gas and melt (Fig. 6a, b) should both
440 evolve with increasing degassing, from S-rich (*early gas* and *early melt*) to Cl-Br rich (*late*
441 *gas* and *late melt*). The *vapour model line* reproduces the observed compositional range of
442 volcanic gas samples from Etna and other mafic systems well (Fig. 6a). Our calculations,
443 therefore, provide a first, though simplistic, reference model to interpret gas-monitoring data
444 from basaltic systems. We propose that high S/Br (along with S/Cl ratios; Aiuppa, 2009) gas
445 compositions reflect shallow degassing of fertile (volatile-rich) magmas in basaltic volcano
446 plumbing systems; while more soluble Cl and Br will prevail in gas released by later
447 degassing stages (e.g., during near-surface syn-eruptive degassing). Our conclusions are
448 opposite to those of Bobrowski and Giuffrida (2012) who, based on observational evidence
449 and use of BrO gas measurements (that under-estimate total Br), proposed that low S/Br ratios
450 mark "deep" degassing episodes of fresh basaltic magmas (at Etna). We stress, instead, that

451 our model calculations more closely reproduce the similar *shallow* degassing behaviour of Cl
452 and Br, which is supported by the limited variability of Cl/Br volcanic gas ratios (Fig 6a). We
453 caution, however, that additional experimental observations, especially at low pressure, and
454 rigorous thermodynamic models, are required to more fully constrain the fate of Br during
455 ascent and degassing of mafic melts.
456 Our *melt model line* also suitably reproduces the compositional trends exhibited by Etna's and
457 Stromboli's melt inclusions (data from Table A.2). Curiously, a set of model calculations
458 initialised as above but with initial volatile contents from Stromboli's most primitive
459 inclusion (ST82c 137; S = 0.2 wt %; Cl = 0.17 wt. %; and Br = 4.8 ppm; Table A.2) output a
460 *melt model line* (black dots) that is virtually indistinguishable from the Etna-like model trend
461 above (Fig. 6b). An additional set of two model lines, calculated using slightly different initial
462 volatiles contents to encompass the whole range of glass inclusion compositions observed, are
463 also illustrated in the Figure 6b (dashed lines).
464
465 *5.3. Bromine contribution of volcanism to the atmosphere*
466 Global compilations show that Br sources and sinks are not strictly balanced, hinting
467 at a missing natural source of Br (Khalil et al., 1993; Montzka et al., 2011). Methyl bromide
468 CH_3Br (mainly produced by marine phytoplankton, biomass burning and fumigants in
469 agriculture) is the largest source of bromine to the atmosphere, and is believed to play a key
470 role in tropospheric and stratospheric ozone depletion (e.g., Mano and Andreae, 1994;
471 Warwick et al., 2006). However, methyl bromide alone cannot explain the total amount of
472 active Br species involved in the ozone destruction process (e.g., Warwick et al., 2006).
473 Following the first detection of bromine monoxide (BrO) in a volcanic plume (Bobrowski et
474 al., 2003), volcanic degassing (both passive and active) has been recognized as a potentially

475 major source of reactive bromine species to the atmosphere (e.g., Gerlach, 2004;
476 Oppenheimer et al., 2006).
477 Possible approaches to quantify the volcanogenic bromine contribution to the atmosphere
478 include: (i) direct measurements from volcanic fumaroles and plumes or (ii) calculation from
479 bromine contents of pre-eruptive melts (i.e., undegassed crystal-hosted melt inclusions).
480 We will apply the second approach to Etna, Merapi and Santorini volcanoes, and compare to
481 direct gas measurements when possible.
482
483 *5.3.1 Bromine emission from an open-vent mafic volcano: the case of Mount Etna*
484 Mount Etna is a persistently degassing basaltic volcano with frequent eruptive activity. We
485 measured the Br contents of olivine-hosted melt inclusions from the trachybasaltic magma
486 erupted during the 2006 Etna eruptions (Table A.2). This eruptive period began in mid-July
487 2006 and continued intermittently for 5 months (Neri et al. 2006; Behncke et al., 2008); it was
488 characterized by strombolian and effusive activity along fissures and at different vent
489 locations and by a short episode of lava fountaining (more details in Behncke et al., 2009 and
490 references therein).
491 Taking into account (i) an average Br content of 6.7 ppm dissolved in the pre-eruptive melt
492 (Table A.2), (ii) a 'dense-rock equivalent' (DRE) erupted volume of 0.012-0.013 km^3
493 (Supplementary Information) and (iii) 25 vol% of phenocrysts (Ferlito et al., 2010), we
494 estimate that 149-169 tons of Br were dissolved in the melt prior to the eruption (SI).
495 The bromine output (as BrO) of this eruptive period, calculated from gas monitoring data
496 (using an average SO_2 flux of 3444 tons/day, from Aiuppa et al., 2008; and a molar volcanic
497 gas BrO/SO_2 ratio of 1.1×10^{-4}; from Bobrowski and Giuffrida, 2012) was 85 tons. However,
498 this is a minimum estimate since BrO is not emitted directly from the magma, but forms by
499 conversion from HBr after emission (e.g. Oppenheimer et al 2006; Martin et al., 2009; von

Glasow, 2010; Roberts et al., 2014). Thermodynamic equilibrium calculations indicate that HBr is the primary Br species at Etnean magmatic temperatures (1050-1100 °C; Aiuppa et al., 2005). The HBr output was unfortunately not determined during the 2006 eruption.

The percentage of BrO of the total emitted bromine is difficult to determine. BrO/SO_2 depends on factors including the plume age (distance from the vent, wind velocity), meteorology, time of day, etc (e.g., Bobrowski and Giuffrida, 2012).

Observations and models suggest that BrO contents may represent 20 to ~50 % of total bromine within a few tens of minutes after plume release (von Glasow, 2010; Roberts et al., 2014), and here we adopt the estimate that BrO comprised 40% of the total bromine emission at Etna (Oppenheimer et al., 2006). Given this assumption, the total mass of bromine emitted during the 2006 Etna eruption was 213 tons, comparable to the mass of bromine in the pre-eruptive melt (149-169 tons, see above and SI), suggesting that Br was efficiently degassed from the melt.

On the basis of the 2006 gas monitoring data encompassing non-eruptive and eruptive periods (i.e., Aiuppa et al., 2005; Bobrowski et al., 2012), we calculate a time-averaged Br emission rate of 0.7 kt/yr (assuming that BrO = 40% of Br total; SI). This is similar to the estimate for the 2004 eruption from Aiuppa et al. (2005). However, as highlighted by Collins et al. (2009), the 2004 and 2006 eruptions were "gas-poor eruptions" thus 0.7 kt/yr should be considered as a minimum Br annual flux for Etna.

5.3.2 Bromine emission from an andesitic volcano: the 2010 Merapi plinian eruption

Merapi volcano (Java, Indonesia) is one of the most active and hazardous volcanoes in the world. The 2010 eruption (VEI 4; Solikhin et al., 2015) was the volcano's largest since 1872. In contrast to the prolonged and effusive dome-forming eruptions typical of Merapi's activity of the last decades, the 2010 eruption began explosively, before a new dome was rapidly

emplaced. This new dome was subsequently destroyed by explosions, generating pyroclastic density currents. The initial explosive phase generated an ash plume that rose to 18 km altitude (Solikhin et al., 2015). The entire eruption released ~0.44 Tg of SO_2 (cumulative SO_2 output based on satellite observations; Surono et al., 2012), much more than previous Merapi eruptions (from 1992 to 2007; Surono et al., 2012). The SO_2 emission rates of the 2010 eruption greatly exceed background and eruptive emissions recorded at Merapi between 1986 and 2007 (Nho et al., 1996; Humaida et al., 2007; Surono et al., 2012). On the basis of the 'petrological method', Surono et al. (2012) and Preece et al. (2014) calculated that the magma volume needed to account for the amount SO_2 released is at least an order of magnitude higher than the estimated DRE volume of magma erupted. They inferred the existence of an exsolved S-rich fluid phase in the pre-eruptive magma body, possibly associated with a deep influx of volatile-rich magma (Costa et al., 2013). According to VolatileCalc modelling by Preece et al. (2014), the vapour phase would have represented 1 wt% of the magma and degassing occurred in closed- (i.e., gas bubbles remained in physical contact and equilibrium with their host melt) rather than in open-system conditions prior to the explosive phase of the 2010 eruption.

The GOME-2 satellite instrument measured SO_2 SCD (slant column densities) of up to 8.9×10^{18} molecules.cm^{-2} (paroxysmal phase of November 5, 2010; Hormann et al., 2013), while BrO/SO_2 ratios were extremely low (8×10^{-6} maximum), indicating that Br was virtually absent. This figure contrasts sharply with the mass of bromine available in the pre-eruptive melt, which our melt inclusions data constrain to be around 433 tons (Supplementary Information). In addition, if we consider the presence a free fluid phase in the reservoir (1 wt%; Preece et al., 2014) and the $D_{Br}^{f/m} = 9.1$ in andesitic melt (Fig. 2b), 73 tons of Br were stored in the fluid and hence immediately available during eruption. Note that we observe the same large discrepancy between the satellite-based estimate of the chlorine yield and the

550 petrological one (see SI). In our opinion, the two most probable explanations are: (1) the
551 paroxysmal phase of the eruption being ash-rich (opacity) and occurring in the middle of the
552 night, the production of BrO was prevented until many hours later (as the reactions are UV-
553 enabled) and is probably lower than in ash-poor plumes (2) satellite instrument measures
554 gases which reached the stratosphere, not what was actually released (bromine might have
555 been scavenged in the troposphere). Additional causes might include: (i) preferential S
556 degassing owing to kinetic factors, (ii) Br uptake by brine saturation during magma uprise,
557 (iii) occurrence of other volatile (e.g. CO_2) which could alter Br partition.
558 The case of Merapi 2010 eruption hints at the need of studies on Br speciation in ash-rich
559 volcanic plumes and additional experimental constraints, in particular on the effect of
560 volatiles other than H_2O on Br systematics.
561
562 *5.3.3. Bromine emission during the cataclysmic Minoan eruption of Santorini volcano*
563 The Late-Bronze age Minoan eruption discharged 38-86 km^3 DRE of rhyodacitic magma (e.g.
564 Pyle, 1990; Johnston et al., 2014). Petrological studies have shown that the pre-eruptive melt
565 was rich in halogens, particularly in chlorine (2500-6000 ppm), and was most probably in
566 equilibrium with an exsolved H_2O-Cl-rich fluid phase (Cadoux et al., 2014; Cadoux et al.,
567 2015; Druitt et al., 2016). Here, we have measured for the first time the Br content of
568 plagioclase-hosted melt inclusions from the Minoan plinian fallout deposit (Table A.2). They
569 give an average value of 7.3 ± 0.8 ppm. Combined with the $D_{Br}^{f/m}$ of 20.2 determined in this
570 study (Fig. 3), we calculate that the pre-eruptive fluid phase contained 147 ppm Br.
571 Assuming a minimum erupted volume of 39 km^3 DRE and a magma crystallinity of 10%, the
572 Minoan pre-eruptive melt would have contained 0.6 Mt of Br. Recent studies have shown
573 that, in silicic magma systems, Br is efficiently degassed with water during eruption (Bureau
574 et al., 2010; Cochain et al., 2015). If we assume that all the Br was degassed from the melt

575 (i.e. we consider 0 ppm of Br in the interstitial melt), the minimum Br output of the Minoan
576 eruption was 0.6 Mt. If we add the contribution of the fluid phase (assuming that it represents
577 5 wt% of the magma mass, as in Cadoux et al., 2015), then the total Br output would have
578 reached 1.3 Mt. These Br yields are consistent with previous estimates of 0.1-1.5 Mt (Cadoux
579 et al., 2015) obtained by multiplying the chlorine yields by the mean molar Br/Cl ratio of
580 0.0022 of volcanic arc gases (Gerlach, 2004).
581 The estimated Br output of this single large explosive event (VEI 6-7) is > 100 times higher
582 than the annual Br flux at a persistently degassing volcano such as the Etna (0.0007 Mt, see
583 before) and the estimated global Br flux at volcanic arcs (0.005-0.015 Mt/yr; Pyle and Mather,
584 2009).
585

586 **6. Conclusions**

587 Determining halogen behaviour in magmatic systems is important to understand their role in
588 biogeochemical cycles and to provide reliable constraints on the contribution of volcanism to
589 the atmosphere and oceans chemistry. The behaviour of the heavier halogens such as Br in
590 magmatic systems is less well understood than that of Cl and F. We have determined the
591 fluid/melt partitioning of bromine at shallow crustal pressure and temperature conditions
592 (100-200 MPa, 900-1200°C) with mafic, intermediate and silicic melts. $D_{Br}^{f/m}$ values range
593 from 5.0 at 100 MPa – 1200°C for the basalt to 20.2 at 200 MPa - 900°C for the rhyodacite.
594 Our data confirm previous experimental constraints on synthetic model magma compositions
595 (Bureau et al., 2000) and allow quantitative modelling of Br behaviour for more mafic melt
596 compositions. The experiments allow first order modelling of S-Cl-Br degassing behaviour in
597 shallow magma reservoirs, permitting a better interpretation of gas-monitoring data. They
598 show also that $D_{Br}^{f/m}$ increases with increasing SiO_2 content of the melt (as for chlorine) and it
599 also appears to be sensitive to melt temperature (increase of $D_{Br}^{f/m}$ as temperature decreases).

600 Overall, our results suggest that the Br yield into atmosphere of cold and silicic magmas will
601 be much larger than that of those which are hotter and more mafic. Our data allow better
602 estimates of the Br yield of past explosive eruptions, provided their pre-eruptive temperature
603 is well known.
604
605 **Acknowledgements**

606 A.C. thanks N. Bouden (CRPG, Nancy) for his assistance during H_2O SIMS measurements,
607 and S. Erdmann (ISTO, Orléans) who provided crystal mounts from Merapi andesite for melt
608 inclusions analysis. N. Metrich (IPGP, Paris) and A. Bertagnini (INGV, Pisa) provided melt
609 inclusions from Stromboli. I. Di Carlo (ISTO, Orléans) and L. Brusca (INGV, Palermo) are
610 acknowledged for their assistance with EMP and LA-ICPMS analyses, respectively This work
611 was supported by the 'Laboratoire d'Excellence VOLTAIRE' (University of Orléans,
612 France), the French agency for research (ANR project #12-JS06-0009-01) and the European
613 Research Council (ERC grant agreement n°305377). A.A., T.A.M. and D.M.P. acknowledge
614 the Diamond Light Source for time on Beamline I18 (Proposal sp8797).
615
616 **References**

617 Aiuppa, A., 2009. Degassing of halogens from basaltic volcanism: insights from volcanic gas
618 observations. Chemical Geology 263, 99-109.
619
620 Aiuppa, A., Giudice, G., Liuzzo, M., Tamburello, G., Allard, P., Calabrese, S., Chaplygin, I.,
621 McGonigle, A.J.S. and Taran, Y. 2012, First volatile inventory for Gorely volcano,
622 Kamchatka, *Geophys. Res. Lett*. 39, L06307
623

624 Aiuppa, A., Baker, D.R., Webster, J.D., 2009. Halogens in volcanic systems. Chemical
625 Geology 263, 1-18.
626
627 Aiuppa, A., Federico, C., Franco, A., Giudice, G., Gurrieri, S., Inguaggiato, S., Liuzzo, M.,
628 McGonigle, A.J.S., Valenza, M., 2005. Emission of bromine and iodine from Mount Etna
629 volcano. Geochemistry, Geophysics, Geosystems 6.
630
631 Aiuppa, A., Federico, C., Paonita, A., Pecoraino, G., Valenza, M., 2002. S, Cl and F
632 degassing as an indicator of volcanic dynamics: the 2001 eruption of Mount Etna. Geophys.
633 Res. Lett. 29-11, doi 10.1029/2002GL015032.
634
635 Aiuppa, A., Giudice, G., Gurrieri, S., Liuzzo, M., Burton, M., Caltabiano, T., McGonigle,
636 A.J.S., Salerno, G., Shinohara, H., Valenza, M., 2008. Total volatile flux from Mount Etna.
637 Geophysical Research Letters 35, L24302, doi:24310.21029/22008GL035871.
638
639 Aiuppa, A., Moretti, R., Federico, C., Giudice, G., Gurrieri, S., Liuzzo, M., Papale, P.,
640 Shinohara, H., Valenza, M., 2007. Forecasting Etna eruptions by real-time observation of
641 volcanic gas composition. Geology 35, 1115–1118.
642
643 Allard, P., La Spina, A., Tamburello, G., Aiuppa, A., Burton, M., Di Muro, A., Staudacher, T.
644 (2011), First measurements of magmatic gas composition and fluxes during an eruption
645 (October 2010) of Piton de la Fournaise hot spot volcano, La Reunion Island. Abstract, 11th
646 Gas Workshop, Commission on the Chemistry of Volcanic Gases (CCVG)-IAVCEI-6, 2011-
647 09 Kamchatka, Russia
648

649 Alletti, M., 2007. Experimental investigation of halogen diffusivity and solubility in Etnean
650 basaltic melts. University of Palermo, Palermo, Italy, p. 92.
651
652 Alletti, M., Baker, D.R., Scaillet, B., Aiuppa, A., Moretti, R., Ottolini, L., 2009. Chlorine
653 partitioning between a basaltic melt and H_2 O–CO_2 fluids at Mount Etna. Chemical Geology
654 263, 37-50.
655
656 Alletti, M., Burgisser, A., Scaillet, B., Oppenheimer, C., 2014. Chloride partitioning and
657 solubility in hydrous phonolites from Erebus volcano: A contribution towards a multi-
658 component degassing model. GeoResJ 3-4, 27-45.
659
660 Baker, D.R., Alletti, M., 2012. Fluid saturation and volatile partitioning between melts and
661 hydrous fluids in crustal magmatic systems: The contribution of experimental measurements
662 and solubility models. Earth-Science Reviews 114, 298-324.
663
664 Baker, D.R., Moretti, R., 2011. Modeling the Solubility of Sulfur in Magmas: A 50-Year Old
665 Geochemical Challenge, Reviews in Mineralogy & Geochemistry. Mineralogical Society of
666 America, pp. 167-213.
667
668 Beermann, O., 2010. The solubility of sulfur and chlorine in H_2 O-bearing dacites of Krakatau
669 and basalts of Mt. Etna. Leibniz Universität Hannover, Germany, Hannover, p. 107.
670
671 Beermann, O., Botcharnikov, R.E., Nowak, M., 2015. Partitioning of sulfur and chlorine
672 between aqueous fluid and basaltic melt at 1050°C, 100 and 200 MPa. Chemical Geology
673 418, 132-157.

Behncke, B., Calvari, S., Giammanco, S., Neri, M., Pinkerton, H., 2008. Pyroclastic density currents resulting from interaction of basaltic magma with hydrothermally altered rock: An example from the 2006 summit eruptions of Mount Etna (Italy). Bull. Volcanol. 70, 1249–1268, doi:1210.1007/s00445-00008-00200-00447.

Behncke, B., Falsaperla, S., Pecora, E., 2009. Complex magma dynamics at Mount Etna revealed by seismic, thermal and volcanological data. J. Geophys. Res. 114, B03211, doi:03210.01029/02008JB005882.

Bobrowski, N., Giuffrida, G., 2012. Bromine monoxide / sulphur dioxide ratios in relation to volcanological observations at Mt. Etna 2006-2009. Solid Earth 3, 433-445.

Bobrowski, N., Hönninger, G., Galle, B., Platt, U., 2003. Detection of bromine monoxide in a volcanic plume. Nature 423, 273–276.

Bobrowski, N., von Glasow, R., Giuffrida, G.B., Tedesco, D., Aiuppa, A., Yalire, M., Arellano, S., Johansson, M., Galle, B., 2015. Gas emission strength and evolution of the molar ratio of BrO/SO_2 in the plume of Nyiragongo in comparison to Etna. Journal of Geophysical Research: Atmospheres 120, 277-291.

Borodulin, G.P., Chevychelov, V.Y., Zaraysky, G.P., 2009. Experimental study of partitioning of tantalum, niobium, manganese, and fluorine between aqueous fluoride fluid and granitic and alkaline melts. Doklady Earth Sciences 427, 868-873.

699 Botcharnikov, R.E., Behrens, H., Holtz, F., Koepke, J., Sato, H., 2004. Sulfur and chlorine
700 solubility in Mt. Unzen rhyodacitic melt at 850°C and 200 MPa. Chem Geol 213, 207-225.
701
702 Botcharnikov, R.E., Holtz, F., Behrens, H., 2007. The effect of CO_2 on the solubility of H_2 O-
703 Cl fluids in andesitic melt. Eur J Mineral 19, 671-680.
704
705 Botcharnikov, R.E., Holtz, F., Behrens, H., 2015. Solubility and fluid-melt partitioning of
706 H_2O and Cl in andesitic magmas as a function of pressure between 50 and 500 MPa. Chem
707 Geol, doi:10.1016/j.chemgeo.2015.1007.1019.
708
709 Bureau, H., Foy, E., Raepsaet, C., Somogyi, A., Munsch, P., Simon, G., Kubsky, S., 2010.
710 Bromine cycle in subduction zones through in situ Br monitoring in diamond anvil cells.
711 Geochimica et Cosmochimica Acta 74, 3839-3850.
712
713 Bureau, H., Keppler, H., Métrich, N., 2000. Volcanic degassing of bromine and iodine:
714 experimental fluid/melt partitioning data and applications to stratospheric chemistry. Earth
715 and Planetary Science Letters 183, 51-60.
716
717 Bureau, H., Métrich, N., 2003. An experimental study of bromine behaviour in water-
718 saturated silicic melts. Geochimica et Cosmochimica Acta 67, 1689-1697.
719
720 Cadoux, A., Iacono-Marziano, G., Paonita, A., Deloule, E., Aiuppa, A., Eby, G.N., Costa, M.,
721 Brusca, L., Berlo, K., Geraki, K., Mather, T.A., Pyle, D.M., Di Carlo, I., 2017. A new set of
722 standards for in-situ measurement of bromine abundances in natural silicate glasses:
723 application to SR-XRF, LA-ICP-MS and SIMS techniques. Chemical Geology 452, 60-70.

Cadoux, A., Scaillet, B., Bekki, S., Oppenheimer, C., Druitt, T.H., 2015. Stratospheric Ozone destruction by the Bronze-Age Minoan eruption (Santorini Volcano, Greece). Scientific Reports 5, 12243.

Cadoux, A., Scaillet, B., Druitt, T.H., Deloule, E., 2014. Magma storage conditions of large Plinian eruptions of Santorini Volcano (Greece). Journal of Petrology 55, 1129-1171.

Carroll, M.R., Webster, J.D., 1994. Solubilities of sulfur, noble gases, nitrogen, chlorine, and fluorine in magmas, in: Carroll, M.R., Holloway, J.R. (Eds.), Volatiles in Magmas. Mineralogical Society of America, pp. 231-279.

Chevychelov, V.Y., Bocharnikov, R.E., Holtz, F., 2008a. Experimental study of chlorine and fluorine partitioning between fluid and subalkaline basaltic melt. Doklady Earth Sciences 422, 1089–1092.

Chevychelov, V.Y., Botcharnikov, R.E., Holtz, F., 2008b. Partitioning of Cl and F between fluid and hydrous phonolitic melt of Mt. Vesuvius at 850-1000 °C and 200 MPa. Chem. Geol. 256, 172–184.

Cochain, B., Sanloup, C., de Grouchy, C., Crépisson, C., Bureau, H., Leroy, C., Kantor, I., Irifune, T., 2015. Bromine speciation in hydrous silicate melts at high pressure. Chemical Geology 404, 18-26.

748 Collins, S.J., Pyle, D.M., Maclennan, J., 2009. Melt inclusions track pre-eruption storage and
749 dehydration of magmas at Etna. Geology 37, 571–574.
750
751 Costa, F., Andreastuti, S., Bouvet de Maisonneuve, C., Pallister, J.S., 2013. Petrological
752 insights into the storage conditions, and magmatic processes that yielded the centennial 2010
753 Merapi explosive eruption. Journal of Volcanology and Geothermal Research 261, 209-235.
754
755 Daniel, J.S., Solomon, S., Portmann, R.W., Garcia, R.R., 1999. Stratospheric ozone
756 destruction: The importance of bromine relative to chlorine. J. Geophys. Res. 104, 23871–
757 23880.
758
759 de Chambost, E., Schumacher, M., Lovestam, G., Claesson, S., 1996. Achieving high
760 transmission with the Cameca IMS 1270, in: Benninghoven, A., Hagenhoff, B., Werner, H.W.
761 (Eds.), Secondary Ion Mass Spectrometry, SIMS X. Wiley, Chichester, pp. 1003-1006.
762
763 Di Carlo, I., Pichavant, M., Rotolo, S.G., Scaillet, B., 2006. Experimental crystallization of a
764 high-K arc basalt: the golden pumice, Stromboli volcano (Italy). Journal of Petrology 47,
765 1317-1343.
766
767 Dolejs, D., Baker, D.R., 2007a. Liquidus equilibria in the system K_2 O-Na_2 O-Al_2 O_3 -SiO_2 -
768 F_2 O_{-1} -H_2 O to 100 MPa: I. Silicate fluoride liquid immiscibility in anhydrous systems. J
769 Petrol 48, 785-806.
770

Dolejs, D., Baker, D.R., 2007b. Liquidus equilibria in the system K_2 O-Na_2 O-Al_2 O_3 -SiO_2 -F_2 O_{-1} -H_2 O to 100 MPa: II. Differentiation paths of fluorosilicic magmas in hydrous systems. J Petrol 48, 807-828.

Druitt, T.H., Mercier, M., Florentin, L., Deloule, E., Cluzel, N., Flaherty, T., Médard, E., Cadoux, A., 2016. Magma Storage and Extraction Associated with Plinian and Interplinian Activity at Santorini Caldera (Greece). Journal of Petrology 57, 461-494.

Edmonds, M., Gerlach, T.M., Herd, R.A., 2009. Halogen degassing during ascent and eruption of water-poor basaltic magma. Chemical Geology 263, 122-130.

Ferlito, C., Viccaro, M., Nicotra, E., Cristofolini, R., 2010. Relationship between the flank sliding of the South East Crater (Mt. Etna, Italy) and the paroxysmal event of November 16, 2006. Bulletin of Volcanology 72, 1179-1190.

Gaillard, F., Scaillet, B., 2014. A theoretical framework for volcanic degassing chemistry in a comparative planetology perspective and implications for planetary atmospheres. Earth and Planetary Science Letters 403, 307-316.

Gennaro M.E. (2017). Sulfur behavior and redox conditions in Etnean hydrous basalts inferred from melt inclusions and experimental glasses. PhD thesis. Università degli Studi di Palermo.

Gerlach, T.M., 2004. Volcanic sources of tropospheric ozone-depleting trace gases. Geochemistry, Geophysics, Geosystems 5, Q09007.

796

797 Hörmann, C., Sihler, H., Bobrowski, N., Beirle, S., Penning de Vries, M., Platt, U., Wagner,
798 T., 2013. Systematic investigation of bromine monoxide in volcanic plumes from space by
799 using the GOME-2 instrument. Atmos. Chem. Phys. 13, 4749-4781.

800

801 Humaida, H., Sumarti, S., Subandriyo, Nandaka, A., Sukarnen, I.G.M., Suharno, Rinekso, K.,
802 Badrijas, Ismai, Sunarto, 2007. Aktivitas Merapi 2006 dan Pemantauan Emisi SO_2 dengan
803 COSPEC, in Erupsi Merapi 2006. Laporan dan Kajian Vulkanisme Erupsi 2006. Departement
804 Energi dan Sumber Daya Mineral, Badan Geologi, Pusat Vulkanologi dan Mitigasi Bencana
805 Geologi.

806

807 Iacono-Marziano, G., Morizet, Y., Le Trong, E., Gaillard, F., 2012. New experimental data
808 and semi-empirical parameterization of H_2 O-CO_2 solubility in mafic melts. Geochimica et
809 Cosmochimica Acta 97, 1-23.

810

811 Johnston, E.N., Sparks, R.S.J., Phillips, J.C., Carey, S., 2014, Revised estimates for the
812 volume of the late Bronze Age Minoan eruption, Santorini. Journal of the Geological Society,
813 London, 171, 583-590.

814

815 Khalil, M.A.K., Rasmussen, R.A., Gunawardena, R., 1993. Atmospheric methyl bromide:
816 Trends and global mass balance. Journal of Geophysical Research: Atmospheres 98, 2887-
817 2896.

818

819 Kutterolf, S., Hansteen, T.H., Appel, K., Freundt, A., Krüger, K., Pérez, W., Wehrmann, H.,
820 2013. Combined bromine and chlorine release from large explosive volcanic eruptions: A
821 threat to stratospheric ozone? Geology 41, 707–710.
822
823 Lesne, P., Scaillet, B., Pichavant, M., 2015. The solubility of sulfur in hydrous basaltic melts.
824 Chemical Geology 418, 104-116.
825
826 Lesne, P., Scaillet, B., Pichavant, M., Beny, J.-M., 2011b. The carbon dioxide solubility in
827 alkali basalts: an experimental study. Contributions to Mineralogy and Petrology 162, 153-
828 168.
829
830 Lesne, P., Scaillet, B., Pichavant, M., Iacono-Marziano, G., Beny, J.-M., 2011a. The H_2 O
831 solubility of alkali basaltic melts: an experimental study. Contributions to Mineralogy and
832 Petrology 162, 133-151.
833
834 Longerich, H.P., Jackson, S.E., Fryer, B.J., Strong, D.F., 1993. The laser ablation microprobe
835 inductively coupled plasma-mass spectrometer. Geoscience Canada 20, 21-27.
836
837 Manõ, S., Andreae, M.O., 1994. Emission of Methyl Bromide from Biomass Burning.
838 Science 263, 1255.
839
840 Martel, C., Pichavant, M., Holtz, F., Scaillet, B., Bourdier, J.-L., Traineau, H., 1999. Effects
841 of fO_2 and H_2O on andesite phase relations between 2 and 4 kbar. J. Geophys. Res. 104,
842 29,453–429,470.
843

844 Martin, R.S., Roberts, T.J., Mather, T.A., Pyle, D.M., 2009. The implications of H_2 S and H_2
845 stability in high-T mixtures of magmatic and atmospheric gases for the production of oxidized
846 trace species (e.g., BrO and NOx). Chem. Geol. 263, 143–150.
847
848 Mather, T.A., Pyle, D.M., Oppenheimer, C., 2003, Tropospheric volcanic aerosol, Geophys.
849 Monogr. 139, 189-212.
850
851 Métrich, N., Allard, P., Spilliardet, N., Andronico, D., Burton, M., 2004. 2001 flank eruption
852 of the alkali- and volatile-rich primitive basalt responsible for Mount Etna's evolution in the
853 last three decades. Earth and Planetary Science Letters 228, 1–17.
854
855 Métrich, N., Bertagnini, A., Di Muro, A., 2010. Conditions of magma storage, degassing and
856 ascent at Stromboli: new insights into the volcano plumbing system with inferences on the
857 eruptive dynamics. J. Petrol. 51, 603-626.
858
859 Métrich, N., Bertagnini, A., Landi, P., Rosi, M., 2001. Crystallisation driven by
860 decompression and water loss at Stromboli volcano (Aeolian Islands). J. Petrol. 42, 1471-
861 1490.
862
863 Métrich, N., Deloule, E., 2014. Water content, δ D and δ 11B tracking in the Vanuatu arc
864 magmas (Aoba Island): Insights from olivine-hosted melt inclusions. Lithos 206-207, 400-
865 408.
866

867 Métrich, N., Wallace, P., 2008. Volatile abundances in basaltic magmas and their degassing
868 paths tracked by melt inclusions, in: Putirka, K., Tepley, F. (Eds.), Minerals, Inclusions and
869 Volcanic Processes. Mineralogical Society of America, pp. 363-402.
870
871 Montzka, S., and Reimann, S. (Coordinating Lead Authors), Engel, A., Krüger, K.,
872 O'Doherty, S., Sturges, W.T., Blake, D., Dorf, M., Fraser, P., Froidevaux, L., Jucks, K.,
873 Kreher, K., Kurylo, M.J., Mellouki, A., Miller, J., Nielsen, O.-J., Orkin, V.L., Prinn, R.G.,
874 Rhew, R., Santee, M.L., Stohl, A., and Verdonik, D., Ozone-depleting substances (ODSs) and
875 related chemicals, Chapter 1 in *Scientific Assessment of Ozone Depletion: 2010*, Global
876 Ozone Research and Monitoring Project–Report No. 52, 516 pp., World Meteorological
877 Organization, Geneva, Switzerland, 2011.
878
879 Moretti, R., Ottonello, G., 2005. Solubility and speciation of sulfur in silicate melts: The
880 Conjugated Toop-Samis-Flood-Grjotheim (CTSFG) model. Geochimica et Cosmochimica
881 Acta 69, 801-823.
882
883 Neri, M., Behncke, B., Burton, M., Galli, G., Giammanco, S., Pecora, E., Privitera, E.,
884 Reitano, D., 2006. Continuous soil radon monitoring during the July 2006 Etna eruption.
885 Geophys. Res. Lett. 33, L24316, doi: 24310.21029/22006GL028394.
886
887 Nho, E.-Y., Le Cloarec, M.-F., Ardouin, B., Tjetjep, W.S., 1996. Source strength assessment
888 of volcanic trace elements emitted from the Indonesian Arc. Journal of Volcanology and
889 Geothermal Research 74, 121–129.
890

Oppenheimer, C., Tsanev, V.I., Braban, C.F., Cox, R.A., Adams, J.W., Aiuppa, A., Bobrowski, N., Delmelle, P., Barclay, J., McGonigle, A.J.S., 2006. BrO formation in volcanic plumes. Geochimica et Cosmochimica Acta 70, 2935-2941.

Preece, K., Gertisser, R., Barclay, J., Berlo, K., Herd, R.A., 2014. Pre- and syn-eruptive degassing and crystallisation processes of the 2010 and 2006 eruptions of Merapi volcano, Indonesia. Contributions to Mineralogy and Petrology 168, 1061.

Pyle, D.M., 1990, New volume estimates for the Minoan eruption, In: Thera and the Aegean World III, vol 2, eds. D Hardy, J. Keller, VP Galanopoulos, NC Flemming and TH Druitt, pp 113-121; The Thera Foundation, London.

Pyle, D.M., Mather, T.A., 2009. Halogens in igneous processes and their fluxes to the atmosphere and oceans from volcanic activity: A review. Chemical Geology 263, 110-121.

Roberts, T.J., Braban, C.F., Martin, R.S., Oppenheimer, C., Adams, J.W., Cox, R.A., Griffiths, P.T., 2009. Modelling reactive halogen formation and ozone depletion in volcanic plumes. Chemical Geology 263, 151-163.

Roberts, T.J., Martin, R.S., Jourdain, L., 2014. Reactive bromine chemistry in Mount Etna's volcanic plume: the influence of total Br, high-temperature processing, aerosol loading and plume–air mixing. Atmospheric Chemistry and Physics 14, 11201-11219.

914 Sawyer, G.M., Salerno, G.G., Le Blond, J.S., Martin, R.S., Spampinato, L., Roberts, T.J.,
915 Mather, T.A., Witt, M.L.I., Tsanev, V.I. and Oppenheimer, C. 2011, Gas and aerosol
916 emissions from Villarrica volcano, Chile, *J. Volcanol. Geotherm. Res*. 203, 62-75.
917
918 Scaillet, B., Evans, B.W., 1999. The 15 June 1991 Eruption of Mount Pinatubo. I. Phase
919 Equilibria and Pre-eruption P-T-*f* O_2 -*f* H_2 O Conditions of the Dacite Magma. Journal of
920 Petrology 40, 381-411.
921
922 Scaillet, B., Holtz, F., Pichavant, M., 1998. Phase equilibrium constraints on the viscosity of
923 silicic magmas: 1. Volcanic-plutonic comparison. Journal of Geophysical Research: Solid
924 Earth 103, 27257-27266.
925
926 Shannon, R.D., 1976. Revised effective ionic radii and systematic studies of interatomic
927 distances in halides and chalcogenides. Acta Cryst. A 32, 751-767.
928
929 Shishkina, T.A., Botcharnikov, R.E., Holtz, F., Almeev, R.R., Portnyagin, M.V., 2010.
930 Solubility of H_2 O- and CO_2 -bearing fluids in tholeiitic basalts at pressures up to 500 MPa.
931 Chemical Geology 277, 115-125.
932
933 Signorelli, S., Carroll, M.R., 2000. Solubility and fluid-melt partitioning of Cl in hydrous
934 phonolitic melts. Geochimica et Cosmochimica Acta 64, 2851-2862.
935
936 Solikhin, A., Thouret, J.-C., Liew, S.C., Gupta, A., Sayudi, D.S., Oehler, J.-F., Kassouk, Z.,
937 2015. High-spatial-resolution imagery helps map deposits of the large (VEI 4) 2010 Merapi
938 Volcano eruption and their impact. Bulletin of Volcanology 77, 20.

939

940 Spilliaert, N., Metrich, N., Allard, P., 2006. S-Cl-F degassing pattern of water rich alkali
941 basalt: modelling and relationship with eruption styles of Mount Etna volcano. Earth Planet.
942 Sci. Lett. 248, 772-786.

943

944 Stelling, J., Botcharnikov, R.E., Beermann, O., Nowak, M., 2008. Solubility of H_2 O- and
945 chlorine-bearing fluids in basaltic melt of Mount Etna at T = 1050-1205°C and P = 200 MPa.
946 Chemical Geology 256, 102-110.

947

948 Surono, Jousset, P., Pallister, J., Boichu, M., Buongiorno, M.F., Budisantoso, A., Costa, F.,
949 Andreastuti, S., Prata, F., Schneider, D., Clarisse, L., Humaida, H., Sumarti, S., Bignami, C.,
950 Griswold, J., Carn, S., Oppenheimer, C., Lavigne, F., 2012. The 2010 explosive eruption of
951 Java's Merapi volcano - A '100-year' event. Journal of Volcanology and Geothermal Research
952 241-242, 121-135.

953

954 von Glasow, R., 2010. Atmospheric chemistry in volcanic plumes. Proceedings of the
955 National Academy of Sciences 107, 6594-6599, doi:6510.1073/pnas.0913164107.

956

957 von Glasow, R., Bobrowski, N., Kern, C., 2009. The effects of volcanic eruptions on
958 atmospheric chemistry. Chemical Geology 263, 131-142.

959

960 Warwick, N.J., Pyle, J.A., Carver, G.D., Yang, X., Savage, N.H., O'Connor, F.M., Cox, R.A.,
961 2006. Global modeling of biogenic bromocarbons. J. Geophys. Res. 111, D24305,
962 doi:24310.21029/22006JD007264.

963

964 Webster, J.D., 1990. Partitioning of F between H_2 O and CO_2 fluids and topaz rhyolite melt.
965 Contrib Mineral Petrol 104, 424-438.
966
967 Webster, J.D., 1992a. Water solubility and chlorine partitioning in Cl-rich granitic systems:
968 Effects of melt composition at 2 kbar and 800°C. Geochimica et Cosmochimica Acta 56, 679-
969 687.
970
971 Webster, J.D., 1992b. Fluid–melt interactions involving Cl-rich granites: experimental study
972 from 2 to 8 kbar. Geochimica et Cosmochimica Acta 56, 679–687.
973
974 Webster, J.D., 2004. The exsolution of magmatic hydrosaline melts. Chem Geol 210, 33-48.
975
976 Webster, J.D., Baker, D.R., Aiuppa, A., 2017. Halogens in Mafic and Intermediate-silica
977 Content Magmas, in: Harlow, D., Aranovich, L.Y. (Eds.), The Role of Halogens in Terrestrial
978 and Extraterrestrial Geochemical Processes: Surface, Crust, and Mantle.
979
980 Webster, J.D., De Vivo, B., Tappen, C., 2003. Volatiles, magmatic degassing and eruptions of
981 Mt. Somma-Vesuvius: constraints from silicate melt inclusions, solubility experiments and
982 modeling, in: De Vivo, B., Bodnar, R.J. (Eds.), Melt Inclusions in Volcanic Systems:
983 Methods, Applications and Problems. Dev Volcanol Elsevier, Amsterdam, pp. 207-226.
984
985 Webster, J.D., Goldoff, B., Sintoni, M.F., Shimizu, N., De Vivo, B., 2014. C-O-H-Cl-S-F
986 volatile solubilities, partitioning, and mixing in phonolitic-trachytic melts and aqueous-
987 carbonic vapor ± saline liquid at 200 MPa. J Petrol 55, 2217-2248.
988

989 Webster, J.D., Holloway, J.R., 1990. Partitioning of F and Cl between hydrothermal fluids
990 and highly evolved granitic magmas, in: Stein, H.J., Hannah, J.L. (Eds.), Ore-bearing granite
991 systems: Petrogenesis and mineralizing processes. Geological Society of America Special
992 Paper, pp. 21-34.
993
994 Webster, J.D., Kinzler, R.J., Mathez, E.A., 1999. Chloride and water solubility in basalt and
995 andesite melts and implications for magmatic degassing. Geochimica et Cosmochimica Acta
996 63, 729-738.
997
998 Webster, J.D., Tappen, C.M., Mandeville, C.W., 2009. Partitioning behavior of chlorine and
999 fluorine in the system apatite-melt-fluid. II: Felsic silicate systems at 200 MPa. Geochimica et
1000 Cosmochimica Acta 73, 559-581.
1001
1002 Webster, J.D., Vetere, F., Botcharnikov, R.E., Goldoff, B., McBirney, A., Doherty, A.L.,
1003 2015. Experimental and modeled chlorine solubilities in aluminosilicate melts at 1 to 7000
1004 bars and 700 to 1250 °C: Applications to magmas of Augustine Volcano, Alaska. American
1005 Mineralogist 100, 522-535.
1006
1007 Webster JD., DR. Baker, A Aiuppa (2017, in press) Halogens in Mafic and Intermediate-
1008 silica Content Magmas. In: The Role of Halogens in Terrestrial and Extraterrestrial
1009 Geochemical Processes: Surface, Crust, and Mantle (D Harlow and L Y. Aranovich, Editors)
1010
1011 Witt, M. L. I., T. A. Mather, D. M. Pyle, A Aiuppa, E. Bagnato, and V. I. Tsanev (2008),
1012 Mercury and halogen emissions from Masaya and Telica volcanoes, Nicaragua, J. Geophys.
1013 Res., 113, B06203, doi:10.1029/2007JB005401

Zajacz, Z., Candela, P.A., Piccoli, P.M., Sanchez-Valle, C., 2012. The partitioning of sulfur and chlorine between andesite melts and magmatic volatiles and the exchange coefficients of major cations. Geochim Cosmochim Acta 89, 81-101.

Figure Captions

Figure 1. Partitioning of bromine between melt and fluid in the run products at T = 1200°C, P_{tot} = 100 MPa and fO_2 ~NNO. The $D_{Br}^{f/m}$ of the basaltic composition, determined by linear regression through the origin, is: 4.95 ± 0.33. The error on the partition coefficient corresponds to the error on the slope of the regression line, as determined by the least squares method.

Figure 2. (a) Melt Br contents versus bulk Br contents (ppm) for the andesitic and rhyodacitic compositions at T = 1060°C, P_{tot} = 200 MPa and fO_2 ~NNO. **(b)** and **(c)** Partitioning of bromine between melt and fluid in the andesitic and rhyolitic run products, respectively, at those conditions. The $D_{Br}^{f/m}$ determined by linear regression through the origin are: 9.1 ± 0.6 for the andesite and 13.9 ± 0.6 for the rhyodacite. The errors on $D_{Br}^{f/m}$ are the errors on the regression lines slope, see Figure 1 caption.

Figure 3. Partitioning of bromine between melt and fluid in the rhyolitic run products, at 900°C, 200 MPa, ~NNO. At lower temperature, the $D_{Br}^{f/m}$ of the rhyodacite increases: 20.2 ± 1.2. Error on $D_{Br}^{f/m}$: see Figure 1 caption. The results are consistent with those of Bureau et al. (2000) on synthetic albitic composition.

Figure 4. $D_{Br}^{f/m}$ as a function of SiO_2 (wt%) of the run products (with [Br°] = 2.4 wt%) of this study. The data for the 900°C – 200 MPa experiment of Bureau et al. (2000) is also plotted. This figure shows the effect of melt composition on $D_{Br}^{f/m}$ and also suggests an effect of the temperature, at least for the more silicic melts

Figure 5. $D_{Br}^{f/m}$ of the rhyodacite composition versus partition experiment temperature (°C).

Figure 6. (a) Triangular plot of S-Cl-Br*300 compositions of volcanic gas samples from selected mafic arc volcanoes. All data refer to near-vent in-situ measurements with filter packs, and are thus representative of gas species SO_2, HCl and HBr (the main S and halogen reservoirs in near-vent plumes, Aiuppa et al., 2005). For comparison, the model-derived compositions of gas coexisting with an Etna-like primitive melt (S: 0.27 wt.%, Cl: 0.18 wt.%, and Br: 5.1 ppm) are shown. These are obtained using the Rayleigh-type open-system equations described in the text. Extent of degassing along both model lines varies from top ("early gas") to bottom ("late gas"). See text for discussion. Volcanic gas data sources: Reunion Island (Indian Ocean): Allard et al (2011); Nyiragongo (Congo): Bobrowski et al. (2015); Hawaii (Pacific Ocean): Mather et al., (2012); Etna (Sicily): Aiuppa et al. (2005), Aiuppa, (2009), Aiuppa, unpublished results; Stromboli (Aeolian Islands): Aiuppa, (2009); Masaya (Nicaragua): Witt et al, (2008); Mount Asama (Japan): Aiuppa, (2009), Aiuppa, unpublished results; Myike-jima (Japan): Aiuppa, (2009), Aiuppa, unpublished results; Gorely (Kamchatka, Russia): Aiuppa et al. (2012); Villarrica (Chile): Sawyer et al., (2011). **(b)** The glass inclusion compositions from Etna and Stromboli (data from Table A.2) are displayed against the model-derived compositions, ranging from S-rich "*early melts*" to halogen-enriched "*late melts*". The melt model line (solid red curve) is derived from the same Etna-like primitive melt composition given above. Some examples of melt model trends obtained with a range of (slightly different) initial volatiles contents are also illustrated. The melt model trend initialized at conditions representative of a Stromboli's primitive melt (S: 0.2 wt %, Cl: 0.17 wt. %, and Br: 4.8 ppm) is depicted by the black dots.

Table Captions

Table 1. Major element composition of the starting dry glasses used for the partitioning experiments.

Table 2. Initial conditions and results of the fluid/melt partitioning experiments.

Table 3. Major element composition (wt%) of the partition experiment products.

Table 1. Major element composition of the starting dry glasses used for the partition experiments

Volcano: Eruption	**Etna: 11/22/2002**		**Santorini: USC-2**		**Santorini: Minoan**	
Sample name	ET02PA27[a]		S09-22[b]		S82-30[c]	
Major oxides (wt%)	*n = 32*	SD	*n = 8*	SD	*n = 22*	SD
SiO_2	47.95	0.82	58.88	0.43	71.24	0.26
TiO_2	1.67	0.11	1.28	0.05	0.45	0.04
Al_2O_3	17.32	0.27	16.16	0.17	14.87	0.15
FeO_{tot}	10.24	0.13	8.18	0.25	2.85	0.18
MnO	0.17		0.20	0.09	0.08	0.05
MgO	5.72	0.28	2.77	0.09	0.73	0.05
CaO	10.85	0.37	6.46	0.12	2.34	0.14
Na_2O	3.42	0.16	4.07	0.15	4.24	0.08
K_2O	1.98	0.10	1.67	0.06	3.08	0.11
P_2O_5	0.51	0.12	0.31	0.06	0.13	0.04

Major elements analyses performed by electron microprobe and recalculated to 100%

a: analysis taken from Iacono-Marziano et al. (2012)

b: Cadoux et al. (2017)

c: Cadoux et al. (2014)

n: number of analyses, and SD: standard deviation of the average of *n* analyses

These dry glasses were also used to synthesize Br standards characterized in Cadoux et al. (2017)

Table 2. Initial conditions and results of the fluid/melt partitioning experiments

	[a]H_2O-NaBr solution mass (g)	[b][Br] calculated in H_2O+NaBr solution (ppm)	[Na] calculated in H_2O+NaBr solution (ppm)	[a]Initial Silicate mass (g)	$[Br]_{melt}$ [c] measured in quenched glass (ppm)	± σ	$[H_2O]$[d] measured in quenched glass (wt%)	[Na] in starting composition (ppm)[e]	[Na] measured in final glass (ppm)[f]	Calculated final mass of glass[g] (g)	Calculated mass of fluid[h] (g)	$[Br]_{fluid}$ (ppm)	$D_{Br}^{f/m}$
Experiment #1 : 1200°C, 100 MPa, ~NNO (2 bars H2), 24 hours													
Run product # (B for basalt)													
M1-B	0.0027	72181	20769	0.0467	3753	168	n.d.	12686	13502	0.0485	0.0009	14298	3.8
Experiment #2 : 1200°C, 100 MPa, ~NNO (2 bars H2), 24 hours													
M2-B	0.0084	142515	41007	0.1006	9112	464	n.d.	12686	13390	0.1038	0.0052	47027	5.2
Experiment #3 : 1200°C, 100 MPa, ~NNO (2 bars H2), 24 hours													
Run product # (B for basalt, A for andesite, RD for rhyodacite)													
M3-B	0.0073	24222	6970	0.0613	2034	290	3.4	12686	13353	0.0635	0.005077	9380	4.6
M3-A	0.0072	24222	6970	0.0622	1912	376	4.8	15097	16543	0.0654	0.004017	12298	6.4
M3-RD	0.0072	24222	6970	0.0623	1426	42	2.9	15727	18175	0.0644	0.005144	16065	11.3
Experiment #4 : 1060°C, 200 MPa, ~NNO (2 bars H2), 48 hours													
M4-A1	0.0070	999	287	0.0625	69.5	0.1	7.2	15097	15245	0.0670	0.002460	948	13.7
M4-A2	0.0070	4968	1430	0.0622	359	48	7.3	15097	15356	0.0668	0.002427	4439	12.3
M4-A3	0.0071	9874	2841	0.0627	733	79	7.3	15097	15282	0.0673	0.002475	8396	11.5
M4-A4	0.0072	24222	6970	0.0624	1960	34	7.2	15097	15468	0.0671	0.002540	16908	8.6
M4-RD1	0.0068	999	287	0.0623	69	10	5.2	15727	16358	0.0656	0.003546	643	9.3
M4-RD2	0.0071	4968	1430	0.0630	240	82	4.9	15727	16729	0.0662	0.003921	4950	20.6
M4-RD3	0.0071	9874	2841	0.0623	591	24	5.4	15727	17211	0.0658	0.003628	8607	14.6
M4-RD4	0.0074	24222	6970	0.0627	1483	242	5.1	15727	16988	0.0661	0.004002	20296	13.7

Table 2. continued

	[a]H_2O-NaBr solution mass (g)	[b][Br] calculated in H_2O+NaBr solution (ppm)	[Na] calculated in H_2O+NaBr solution (ppm)	[a]Initial Silicate mass (g)	$[Br]_{melt}$ [c] measured in quenched glass (ppm)	± σ	$[H_2O]$[d] measured in quenched glass (wt%)	[Na] in starting composition (ppm)[e]	[Na] measured in final glass (ppm)[f]	Calculated final mass of glass[g] (g)	Calculated mass of fluid[h] (g)	$[Br]_{fluid}$ (ppm)	$D_{Br}^{f/m}$
Experiment #5 : 900°C, 200 MPa, ~NNO (2 bars H2), 92 hours													
M5-RD1	0.0073	999	287	0.0623	79	6	6.8	15727	16358	0.0665	0.003050	677	8.6
M5-RD2	0.0069	4968	1430	0.0621	226	31	6.0	15727	16729	0.0659	0.003089	6285	27.9
M5-RD3	0.0072	9874	2841	0.0633	608	97	6.5	15727	17211	0.0675	0.002976	10089	16.6
M5-RD4	0.0072	24222	6970	0.0632	1251	214	5.6	15727	16988	0.0669	0.003486	26017	20.8

a: loaded into capsule

b: bulk Br referred as [Br°] in the text and figures

c: [Br] determined by LA-ICP-MS in glasses from experiments #1 and 2 (average of 3 to 10 analyses per charge)
[Br] determined by SIMS in glasses from experiments #3 to 5 (3 to 6 analyses per charge)

d: H_2Omelt not determined in run products from exp. #1 and 2. H_2Omelt in run products from exp. #3 to 5 determined by SIMS (5-7 analyses per charge)

e: from Table 1

f: from Table 3

g: For exp. #1 and 2 this mass was determined by weighing the charge after piercing of the capsule and evaporation in the oven at 120°C overnight to allow fluid to escape. It was calculated for exp. #3 to 5 by the sum of the initial silicate weighed into the capsule and the final calculated mass of Br and H_2O incorporated into it. This method was preferred for the more evolved compositions to take account of the potential presence of fluid trapped as fluid inclusions within the glass (e.g. in rhyodacitic glassy products, Fig. A.1)

h: For exp. #1 and 2 fluid mass was determined by subtracting the weight after piercing and evaporation in the oven at 120°C overnight from the original mass loaded into the capsule. It was calculated for exp. #3 to 5 by the difference between the total weighed into the capsule and the final calculated mass of the glass with Br and H_2O incorporated into it.

Table 3. Major element composition (wt%) of the partitioning experiment glassy products

Experiment #	**1**		**2**		**3**						**4**							
Product ID	M1-B		M2-B		M3-B		M3-A		M3-RD		M4-A1		M4-A2		M4-A3		M4-A4	
	n = 10	SD	*n = 10*	SD	*n =7*	SD	*n = 7*	SD	*n = 6*	SD	*n = 6*	SD	*n = 6*	SD	*n = 6*	SD	*n = 6*	SD
SiO_2	50.23	0.37	48.36	0.29	48.96	0.59	59.54	0.30	71.31	0.30	59.50	0.33	59.52	0.38	59.70	0.43	59.44	0.54
TiO_2	1.83	0.09	1.75	0.09	1.65	0.16	1.27	0.14	0.40	0.06	1.28	0.14	1.36	0.17	1.33	0.18	1.38	0.11
Al_2O_3	16.88	0.18	16.34	0.15	16.55	0.19	16.32	0.20	14.77	0.18	16.37	0.13	16.45	0.28	16.55	0.10	16.27	0.18
FeO_{tot}	10.44	0.32	9.89	0.30	9.12	0.38	7.36	0.29	2.15	0.15	7.66	0.41	7.50	0.39	7.19	0.22	7.73	0.19
MnO	0.18	0.10	0.17	0.09	0.17	0.12	0.10	0.08	0.10	0.12	0.19	0.08	0.18	0.09	0.20	0.14	0.28	0.09
MgO	6.56	0.20	6.35	0.17	6.65	0.05	2.74	0.06	0.72	0.03	2.73	0.09	2.68	0.08	2.66	0.05	2.71	0.05
CaO	11.22	0.25	11.01	0.31	10.82	0.26	6.33	0.14	2.40	0.08	6.35	0.06	6.35	0.09	6.31	0.11	6.34	0.14
Na_2O	3.64	0.16	3.61	0.12	3.60	0.10	4.46	0.08	4.90	0.09	4.11	0.09	4.14	0.11	4.12	0.05	4.17	0.09
K_2O	2.05	0.14	1.92	0.21	2.07	0.20	1.66	0.07	3.20	0.10	1.59	0.06	1.56	0.07	1.61	0.10	1.51	0.05
P_2O_5	0.61	0.08	0.60	0.09	0.40	0.12	0.21	0.15	0.07	0.06	0.22	0.12	0.27	0.15	0.31	0.18	0.16	0.20

1077

1078

Table 3. continued

Experiment #	**4**								**5**							
Product ID	M4-RD1		M4-RD2		M4-RD3		M4-RD4		M5-RD1		M5-RD2		M5-RD3		M5-RD4	
	n = 6	SD	*n = 5*	SD	*n = 6*	SD	*n = 7*	SD	*n = 8*	SD	*n = 8*	SD	*n = 9*	SD	*n = 7*	SD
SiO_2	71.77	0.26	71.48	0.73	71.49	0.61	71.68	0.37	71.56	0.31	71.47	0.39	71.50	0.31	71.31	0.52
TiO_2	0.51	0.04	0.48	0.09	0.46	0.07	0.45	0.08	0.49	0.08	0.42	0.10	0.46	0.10	0.41	0.11
Al_2O_3	14.85	0.20	14.92	0.05	15.05	0.19	14.63	0.22	14.49	0.29	14.40	0.21	14.39	0.13	14.44	0.22
FeO_{tot}	2.18	0.28	2.35	0.12	2.28	0.25	2.40	0.21	2.88	0.21	3.01	0.30	2.96	0.19	2.89	0.20
MnO	0.14	0.05	0.05	0.05	0.08	0.11	0.09	0.07	0.06	0.08	0.08	0.08	0.07	0.07	0.05	0.06
MgO	0.69	0.04	0.69	0.04	0.66	0.02	0.71	0.04	0.71	0.03	0.70	0.05	0.72	0.04	0.71	0.04
CaO	2.47	0.07	2.46	0.07	2.45	0.11	2.37	0.06	2.34	0.08	2.41	0.11	2.37	0.06	2.38	0.09
Na_2O	4.41	0.34	4.51	0.07	4.64	0.09	4.58	0.10	4.35	0.08	4.41	0.08	4.45	0.14	4.58	0.09
K_2O	2.88	0.19	2.86	0.13	2.83	0.11	2.90	0.10	3.01	0.19	2.97	0.12	3.00	0.19	3.07	0.17
P_2O_5	0.10	0.06	0.19	0.10	0.05	0.08	0.18	0.09	0.11	0.06	0.11	0.10	0.09	0.10	0.16	0.05

Major element analyses recalculated to 100%

n is the number of analyses per product, SD is the standard deviation on the average of *n* analyses

1079

1080

1081 **Figure 1**

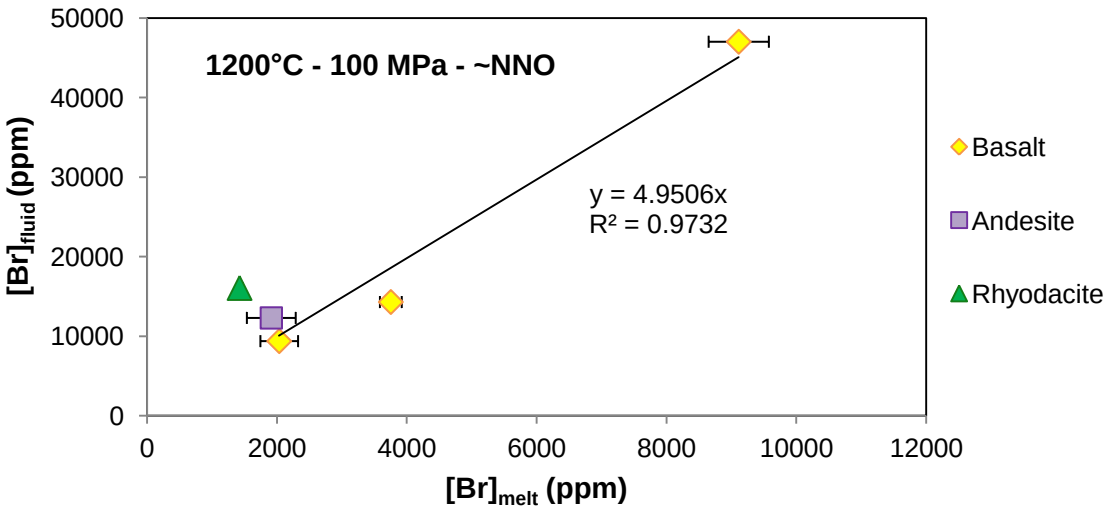

1082

1083

Figure 2 (a)

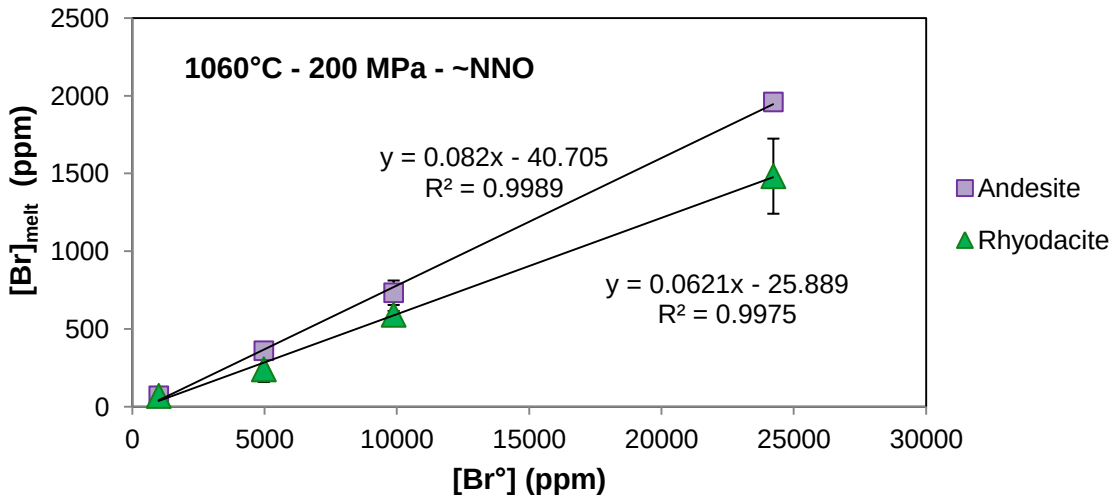
1060°C - 200 MPa - ~NNO
y = 0.082x - 40.705
R² = 0.9989
y = 0.0621x - 25.889
R² = 0.9975
Andesite
Rhyodacite
[Br]melt (ppm)
[Br°] (ppm)
0
500
1000
1500
2000
2500
0
5000
10000
15000
20000
25000
30000

(b)

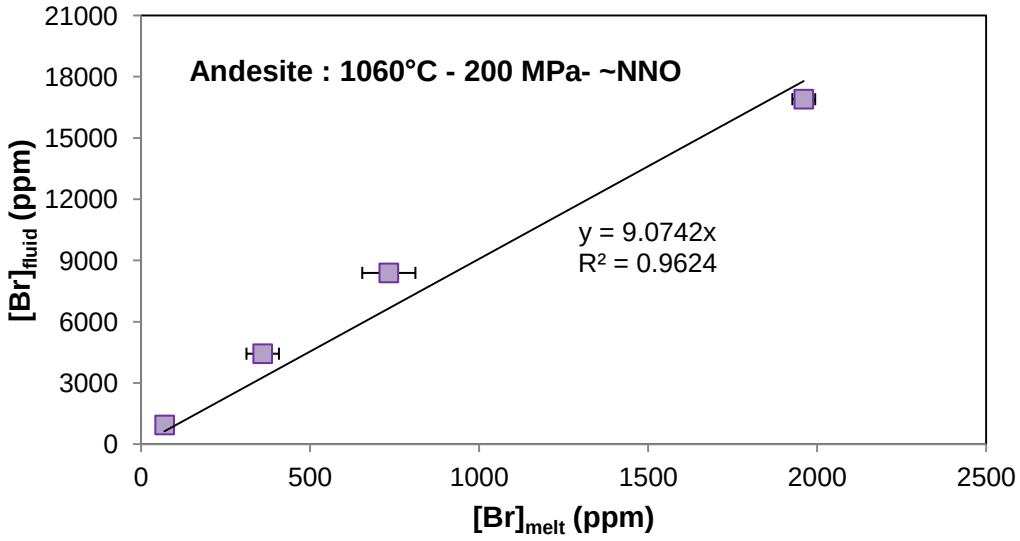
Andesite : 1060°C - 200 MPa- ~NNO
y = 9.0742x
R² = 0.9624
[Br]fluid (ppm)
[Br]melt (ppm)
0
3000
6000
9000
12000
15000
18000
21000
0
500
1000
1500
2000
2500

(c)

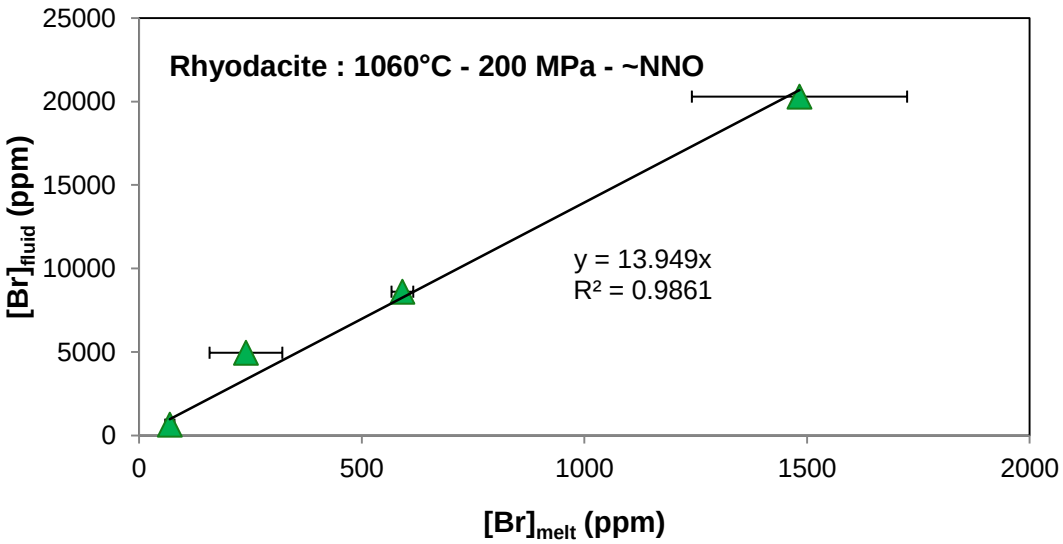
Rhyodacite : 1060°C - 200 MPa - ~NNO
y = 13.949x
R² = 0.9861
[Br]fluid (ppm)
[Br]melt (ppm)
25000
20000
15000
10000
5000
0
0
500
1000
1500
2000

1097 **Figure 3**

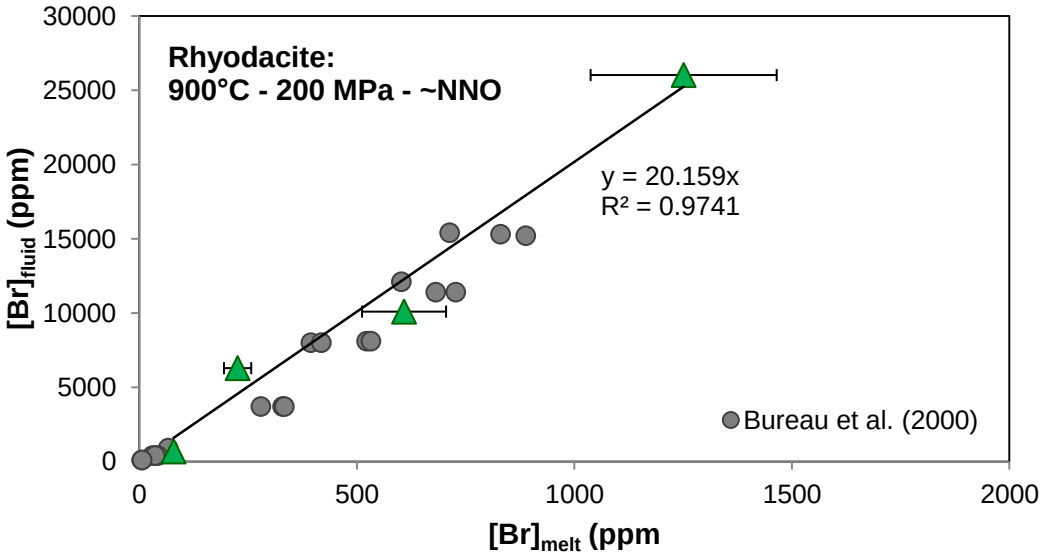

1098

1099

Figure 4

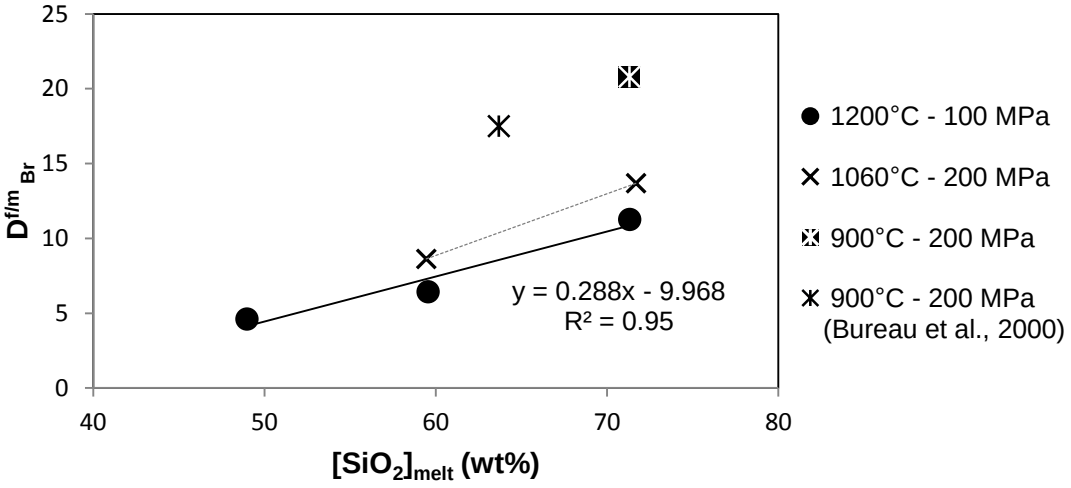
25
20
15
10
5
0
40
50
60
70
80
$D^{f/m}_{Br}$
$[SiO_2]_{melt}$ (wt%)
y = 0.288x - 9.968
R² = 0.95
1200°C - 100 MPa
1060°C - 200 MPa
900°C - 200 MPa
900°C - 200 MPa
(Bureau et al., 2000)

1103 **Figure 5**

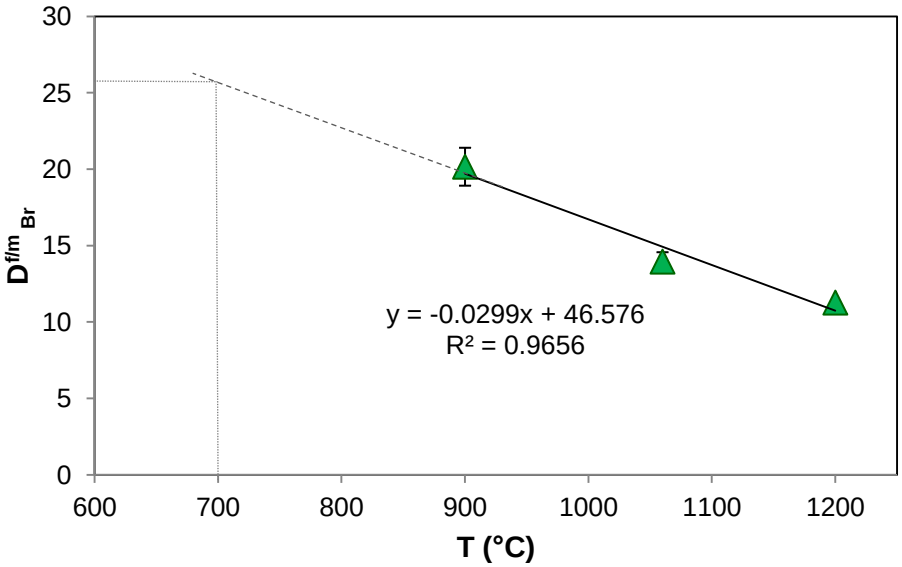

1104

1105

1106 **Figure 6**

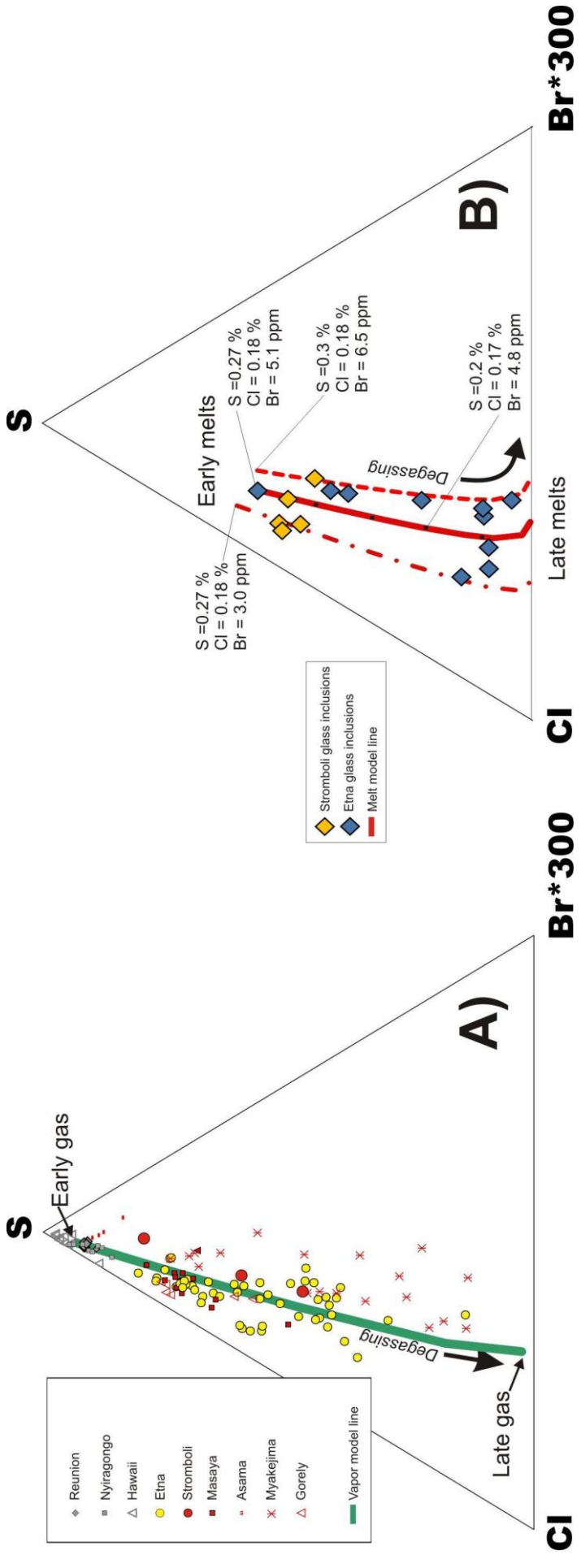

Supplementary material for online publication only

Click here to download Supplementary material for online publication only: Supplementary Info_31-10-17.docx

Supplementary material for online publication only

Click here to download Supplementary material for online publication only: Figure A.1.pdf

Supplementary material for online publication only

Click here to download Supplementary material for online publication only: Supplementary Tables.xlsx